FULL PAPER

Titanium-based tetrakis-2,3-[5,6-di(substituted)pyrazino]porphyrazine: synthesis and characterization

Polyssena Renzi,[a]* Lucia Mazzapioda,[a] Francesca Nardelli,[b] Francesca Martini,[b] Marco Geppi,[b] Carmine Mancone,[c] Maria Assunta Navarra,[a] Francesca D'Acunzo,[d] Patrizia Gentili,[a]

[a] Dr P. Renzi, Dr L. Mazzapioda, Prof. P. Gentili, Dr M. A. Navarra
Department of Chemistry
Sapienza Università di Roma
P.le A. Moro 5, 00185 Rome, Italy
E-mail: polyssena.renzi@uniroma1.it
[b] Dr F. Nardelli, Dr F. Martini, Prof. M. Geppi
Department of Chemistry and Industrial Chemistry
University of Pisa
Via G. Moruzzi 13, 56124, Pisa, Italy
[c] Prof. C. Mancone
Department of Molecular Medicine
Sapienza University of Rome
Viale Regina Elena 291, 00161 Rome, Italy
[d] Dr. F. D'Acunzo
Consiglio Nazionale delle Ricerche
Istituto per I Sistemi Biologici
Sezione Meccansimi di Reazione
c/o Department of Chemistry
Sapienza Università di Roma
P.le A. Moro 5, 00185 Rome, Italy

Supporting information for this article is given via a link at the end of the document.

Abstract: Tetrapyrazinoporphyrazine (TPysPz) ligands and metal complexes find, generally, application as electronic materials and catalysts. Considering the limited application of Titanium (Ti), we prepared and characterized a family of ligands and Ti-based complexes of tetrakis-2,3-[5,6-di-R_8-pyrazino]porphyrazine (R= H, 2-Py, Ph). UV-Vis measurements in different solvents confirmed molecular aggregation, which resulted more pronounced in the presence of 2-pyridil and phenyl substituents on the macrocycle edge. Because of low solubility, solid state NMR was applied for structure characterization. Additional IR, MALDI-TOF and SEM analyses were carried out to complete the characterization. Cyclic voltammetry in DMSO/Bu_4NBF_4 0.1 M unveiled that our Ti-complexes can take part in up to five redox events. The first two involved quasi-reversible Ti(IV) reduction followed by two or three reduction at the expense of the TPysPz macrocycle. To test the applicability of our compounds as catalytic materials, we performed a preliminary cyclic voltammetry investigation in the solid-state, which showed typical peaks of hydrogen redox reactions.

Introduction

Azaanalogues of phthalocyanines, tetrapyrazinoporphyrazines (TPysPzs) ligands and metal complexes have seen a rapid development in the last three decades. Ranging from electronic materials to photodynamic therapy and catalysis, a plethora of applications has been documented in the literature for these compounds.[1-2] Interestingly, the introduction of different substituents in the periphery of the macrocycle is able to tune its properties, activity and solubility in organic or aqueous media. As reported in the literature, several metals (Mg, Zn, Cu, Ni, Fe, Co, Si) can be coordinated by TPysPzs. Among them, Titanium (Ti) has been seldom employed in the template synthesis of tetrapyrazinoporphrazine metal complexes,[3] despite its abundance in the Earth's crust and its similarity in ionic radius and coordination chemistry with iron (Fe^{III}).[4-6] In general, in oxidizing atmosphere, titanium exists as Ti(IV) and it can be coordinated by tetrapyrrole ligands as a titanyl unit (TiO^{2+}).[7-10]

In this paper, we present the synthesis and the characterization of a series of ligands and Ti-based complexes of tetrakis-2,3-[5,6-di-R_8-pyrazino]porphyrazine (R= H, 2-Py, Ph). For all the compounds (**2a-c** and **3a-c**, Scheme 1) synthesized a full characterization from the spectroscopic and electrochemical point of view is presented. Aggregation behavior was highlighted by UV-Vis spectroscopy, while cyclic voltammetry was employed to unveil the presence of differences in the redox behavior between Ti-based complexes **3a-c**, the corresponding ligands **2a-c** and similar metal complexes of TPysPzs previously described in literature.

The interest towards compounds **3a-c** arises from the potentiality of applying these molecules as catalysts in oxygen reduction reaction (ORR),[11-12] as dyes in dye sensitized solar cells (DSSC),[13-15] and in the detection of hydrogen peroxide.[16] Indeed, the increasing energy demand connected with the replacement of fossil fuels and environmental concerns has made necessary the development of advanced and next-generation technologies for energy production. Among the approaches pursued to enhance these processes, the use of catalysts revealed to be the most effective. Although porphyrin, corrole and phtalocyanine-based

ligands can be a valid alternative,[11-12] their synthesis is frequently characterized by low yields, a feature which can hamper their production on industrial scale. While the proof of concept has been demonstrated, the potentiality of tetrapyrazinoporphyrazines derivatives has still to be explored.

Results and Discussion

Preparative Aspects.

As reported in the Experimental section and in the Supporting Information, ligands **2a-c** and complexes **3a-c** can be prepared from the common starting-materials **1a-c** (Scheme 1). The synthesis of **1a-c** was accomplished by modifying the procedure reported by Mørkved employing diaminomaleonitrile and an α-diketone as starting-material in glacial acetic as solvent (**1a**: 76% yield; **1b**: 73% yield; **1c**: 85% yield).[17] The solids obtained were purified by extraction and washing with water, brine and saturated solutions of $NaHCO_3$, and crystallized from water/ethanol prior to use. Pyrazinoporphyrazine macrocycles **2a-c** were prepared according to the procedure reported by Ercolani, Kadish *et al.* by autocyclotetramerization of **1a-c** at high temperatures (from 175°C to 240°C according to **1a-c** melting-point) in the presence of DBU as catalyst (**2a**: 21% yield; **2b**: 20% yield; **2c**: 18% yield).[18-19] While the ligand synthesis could be realized without paying specific attention to the water content, the synthesis of the complex needed the application of Schlenk technique and stringent dry reaction conditions in the presence of an excess of **1a-c** in order to avoid the formation of titanium dioxide (TiO_2). The Ti-complex was obtained by melting the starting-material **1a-c** and subsequently adding titanium (IV) butoxide against a stream of inert gas. The reaction was kept at high temperature for 5 hours, then the greenish/bluish solids **3a-c** were purified by washing with MeOH and/or CH_2Cl_2 in order to remove the contaminants. The solids were collected each time by centrifugation and dried under vacuum to constant weight (**3a**: 78% yield; **3b**: 65% yield; **3c**: 95% yield).

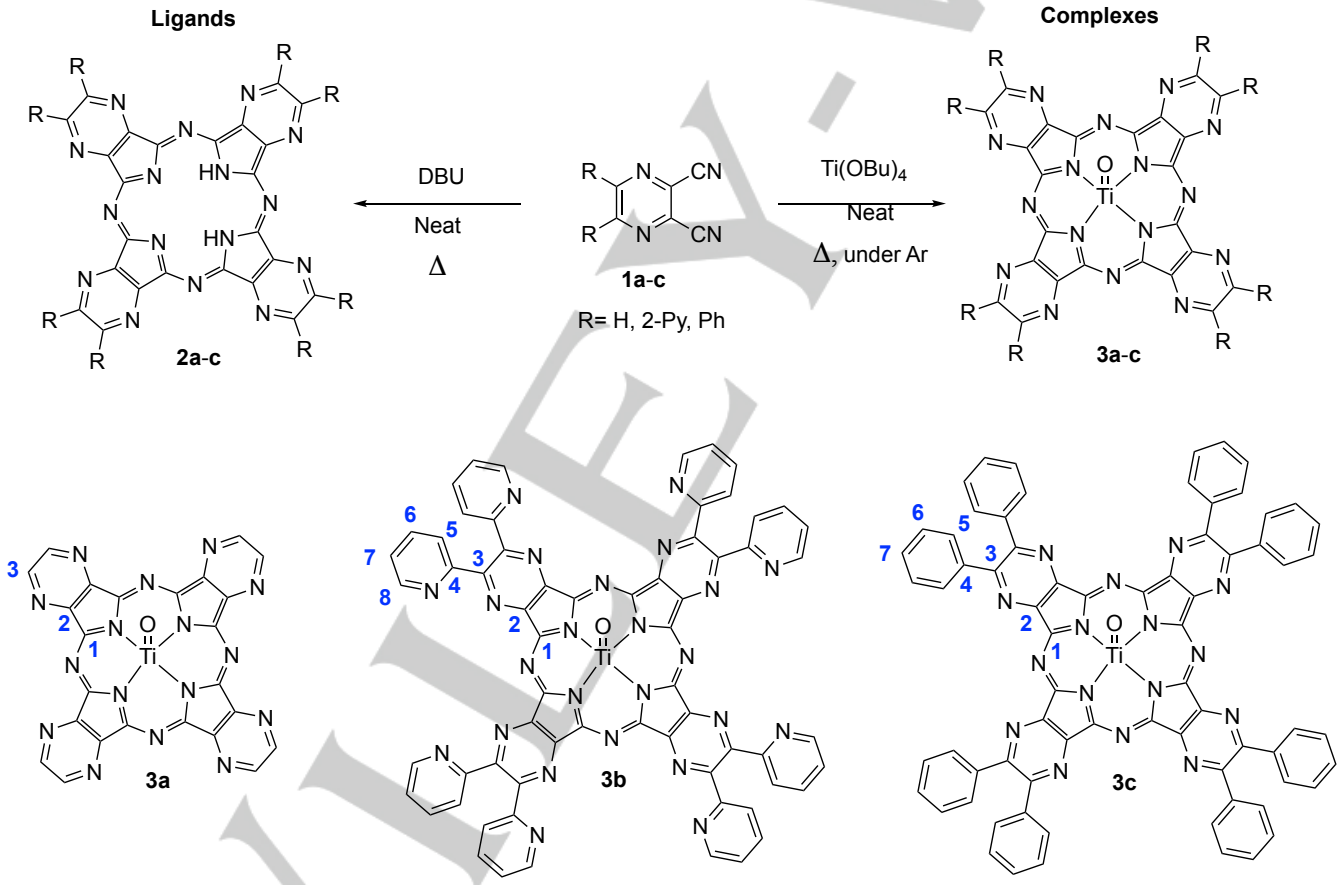

Scheme 1. Reaction scheme for the synthesis of ligands **2a-c** and Ti-based complexes of tetrakis-2,3-[5,6-di-R_8-pyrazino]porphyrazine (R= H, 2-Py, Ph) **3a-c**. Numbers in blue will be useful in the assignment of the ^{13}C-SSNMR spectra reported in Figure 6.

Solution Studies: UV-Vis Spectra.

The UV-vis spectral behavior of Titanium-based complexes **3a-c** was studied as a function of time in dimethylformamide (DMF), a polar aprotic solvent, and in methylenchloride (CH_2Cl_2), a nondonor solvent. All complexes yielded clear solution in both solvents, and the formation of colloidal suspensions as described by Donzello *et al.* for similar compounds was not observed.[18-19] A greater solubility was obtained in DMF than in CH_2Cl_2.

Furthermore, changes in the intensities of the UV-vis absorptions could be observed as a function of time (Figure 1). This behavior can be ascribed to molecular aggregation both in the form of intermolecular association or dissociation upon time. Complexes **3a**-**c** showed a different response depending on the solvent employed. In general, in CH_2Cl_2 the spectra were characterized by an increase of Q and B bands with time (Figure 1) reaching their maximum intensities after one hour. These spectral changes can be attributed to intermolecular dissociation ending with the formation of monomeric macrocyclic units in keeping with previous results.[18-19]

The same behavior was shown by complex **3a** in DMF. In contrast, the UV-vis spectra of compounds **3b** and **3c** in the same solvent were characterized by a progressive increase in the absorption, respectively at 761 and 759 nm, with a simultaneous decrease in the Q and B band intensities. If disaggregation could be obtained for all compounds in the nondonor solvent, CH_2Cl_2, and for compound **3a** in DMF, the introduction of aromatic substituents such as 2-pyridil (complex **3b**) and phenyl groups (complex **3c**) caused an intensification of the aggregation phenomena. These could be potentially due to an increase in the π-π stacking interactions between the Titanium-based complex monomers reaching its maximum after one hour. The UV-vis spectra in DMF are characterized by intense and sharp peaks in the Q-region respectively at 647 (**3a**), 667 (**3b**) and 665 (**3c**) nm (Figure 1 and Table 1).

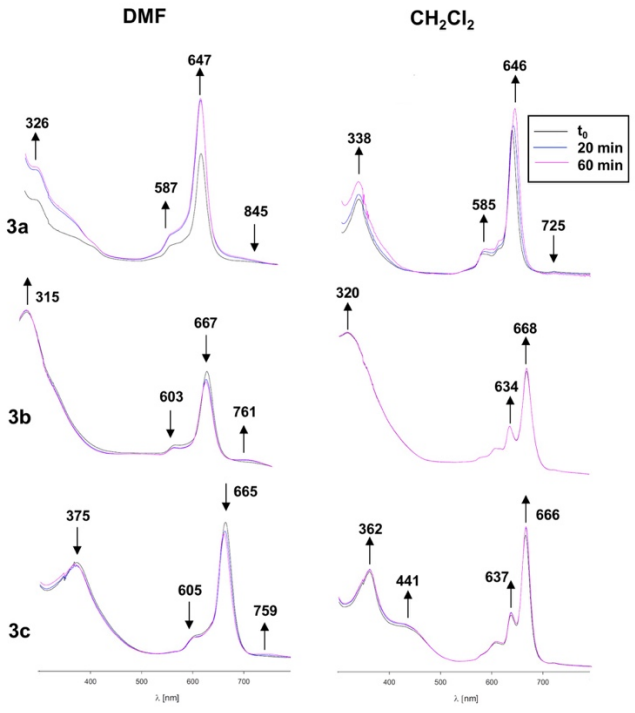

Figure 1. UV-vis spectral changes of Titanium-based complexes **3a**-**c** in DMF and CH_2Cl_2 solutions as a function of time.

Generally, a negligible solvent effect was observed in the Q band position, while the B band was subjected to a red-shift for complexes **3a**-**b** and to a blue-shift for complex **3c** changing the solvent from DMF to CH_2Cl_2. A summary of **3a**-**c** absorptions, together with a comparison with the corresponding ligands **2a**-**c** is presented in Table 1. In particular, the introduction of eight 2-pyridil (**3b**) or eight phenyl groups (**3c**) caused a bathochromic shift in the Q band respectively of 20 nm (for complex **3b** in CH_2Cl_2 the shift is of 22 nm) and 18 nm (for complex **3c** in CH_2Cl_2 the shift is of 20 nm) in DMF with respect to the non-substituted complex **3a**. These shifts are quite small because only a partial conjugation between the substituents and the macrocycle framework is possible due to intrinsic steric hindrance of 2-pyridil and phenyl groups.

Weak vibrational bands were present between 587 and 605 nm. These peaks became more intense in CH_2Cl_2 for compounds **3b** and **3c** (peaks at 603 and 667 nm), while for complex **3a** the peak at 585 nm remained broad. The splitting in the Q band in CH_2Cl_2 has been observed for other metal complexes in chlorinated solvents and it is probably due the formation of excitonic coupling because of molecular association.[20]

Finally, as observed for porphyrazines and phthalocyanines, because of HOMO-LUMO π-π^* transitions, B bands between 315 and 421 nm are also present (Table 1).

As it can be seen from Table 1, the UV-vis spectra of compounds **3a**-**c** strictly parallel the ones of the corresponding un-metallated macrocycles, with the exception in the B band region. As shown in Figure 2, ligands were, generally, characterized by an envelope in the 300-400 nm region, whereas the corresponding metallated compound presented more defined and red-shifted absorptions. In contrast to complex **3a**, ligand **2a** presented a very low solubility in both DMF and CH_2Cl_2 (see Figure 2a for a comparison between **2a** and **3a**), while more soluble ligands were obtained by the introduction of 2-pyridil and phenyl groups (Figure 2b).

Table 1. UV-Vis spectral data for ligands **2a**-**c** and complexes **3a**-**c** in different solvents.

Compound	Solvent	B band region [nm]	Q band region [nm]
2a	DMF	404 435 576	636
3a	DMF	326 587	647
3a	CH_2Cl_2	338 585	646
2b	CH_2Cl_2	355 421 581	617 634 668
3b	DMF	315	603 667
3b	CH_2Cl_2	320 577	634 668
2c	DMF	336	657
2c	CH_2Cl_2	342	638 667
3c	DMF	375	605 665
3c	CH_2Cl_2	362 441	607 637 666

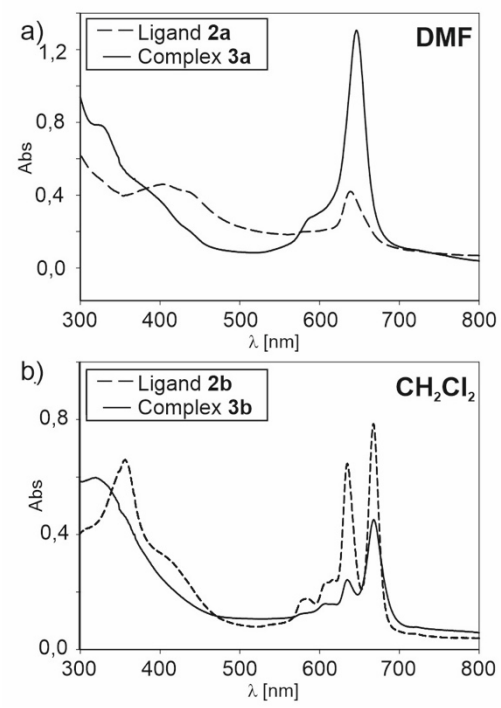

Figure 2. Comparison between the UV-vis spectra of ligands **2a**-**b** and complexes **3a**-**b** in different solvents.

Electrochemical Measurements.

As proposed in literature for tetra-2,3-pyrazinoporphyrazines ligands/metal complexes and for phatholocyanine and diazepinoporphyrazine analogues, the macrocycle is able to give four one-electron reductions in the range of potentials 0.0 ÷ -2.0 V *vs* SCE. In general, cyclic voltammograms (CVs) of ligands present, also, a fifth redox event which has been attributed to the reduction of a dianionic specie in equilibrium with the neutral porphyrazine as confirmed by the measurements in pyridine. In the case of cobalt-based complexes, two reductions on charge of Co^{II} occur prior to the classical four-reduction sequence observed for Cu^{II}, Zn^{II} and Mg^{II} complexes.

Cyclic voltammograms of complexes **3a-c** in DMSO and DMF containing Bu_4NBF_4 0.1 M as support electrolyte are shown in Figures 3 and 4. Scan rates of 0.5 V/sec were employed for each measurement. Even though, a suspended excess of compound was employed well defined redox processes were observed, only, for complex **3a** in both solvents, particularly in DMSO. The quality of voltammograms in DMF was strongly affected by the poor solubility of compounds **3b**-**c**. On the other hand, low intensity redox events were clearly identified in DMSO for all three compounds. In general, no oxidations were observed up to a positive potential of 1.1 V *vs* SCE (The complete set of voltammograms recorded is summarized in the Supporting Information).

The voltammogram in DMSO of ligand **2a** showed only one reversible peak at -0.77 V (Figure 3), probably due to the reduction of dianion $\mathbf{2a}^{2-}$. This result is in agreement with the literature[18-19, 21] where tetrapyrazinoporphyrazines are known to undergo deprotonation upon dissolution in DMSO and their dianion $TPysPzs^{2-}$ are in equilibrium with the neutral forms $TPysPzsH_2$. In contrast, the CV of **2a** in DMF/CH_2Cl_2 5/1 showed one irreversible peak at -0.89 V for the reduction of the corresponding dianion and a second reversible peak, barely visible, at -1.42 V, which can be probably attributed to the reduction of its neutral form (Figure 3).[22]

As shown in Figure 3 and 4, complex **3a** exhibits in DMSO five redox couples labeled I – V. In the case of couples I – IV, the cathodic to anodic peak separation ($\Delta E = E^p_c - E^p_a$) at 0.5 V/s was in the range 85 – 100 mV; however the cathodic to anodic peak current ratios (I_{pc}/I_{pa}) were near unit, suggesting a *quasi-reversible* behavior. The CV of **3a** in DMF, **3b** and **3c** in DMSO showed a similar electrochemical behavior, although peaks were not cleanly resolved (Figures 3-4).

The half-wave potentials ($E_{1/2}$) and the potential separation between different stepwise reductions (Δ) are reported in Table 2 for **3a-c** complexes. For comparison, $E_{1/2}$ and Δ of ligand **2b**/metal M^{II} cations complexes (**2b**-M^{II})[23] and tetra-substituted oxo(phthalocyaninato)titanium(IV) complexes [$(PhCH_2O)_4Pc$-$Ti^{IV}O$ and $(PhOC_6H_4OCH_2)_4Pc$-$Ti^{IV}O$][24] are reported in the same Table.

As shown in Table 2, the $E_{1/2}$ and the potential separation between couples III, IV and V for compounds **3a-c** are very similar to those of metal complexes **2b**-M^{II}; as proposed in literature, these stepwise reduction sequences are assumed to be ligand-centered. Moreover, the new titanium-based tetrapyrazinoporphrazine complexes are reduced more easily than their analogues $(PhCH_2O)_4Pc$-$Ti^{IV}O$ and $(PhOC_6H_4OCH_2)_4Pc$-$Ti^{IV}O$ thanks to the substitution of benzene rings in phthalocyanines with pyrazine rings. It has been demonstrated that the sequence of reduction process for oxotitanium tetra-substituted phthalocyanines complexes involved two initial metal-centered $Ti^{IV} \rightarrow Ti^{III}$ and $Ti^{III} \rightarrow Ti^{II}$ stepwise reductions, followed by two other ligand-based reduction steps.[24] From all these observations we propose the following mechanism for the reduction of compounds **3a-c** (Scheme 2):

$$[TPyzPz\text{-}Ti^{IV}] + e \leftrightarrows [TPyzPz\text{-}Ti^{III}]$$

$$[TPyzPz\text{-}Ti^{III}] + e \leftrightarrows [TPyzPz\text{-}Ti^{II}]$$

$$[TPyzPz\text{-}Ti^{II}] + e \leftrightarrows [TPyzPz\text{-}Ti^{II}]^-$$

$$[TPyzPz\text{-}Ti^{II}]^- + e \leftrightarrows [TPyzPz\text{-}Ti^{II}]^{2-}$$

$$[TPyzPz\text{-}Ti^{II}]^{2-} + e \leftrightarrows [TPyzPz\text{-}Ti^{II}]^{3-}$$

Scheme 2. Suggested mechanism for reduction of complexes **3a**-**c**.

In other words, as suggested by cyclic voltammetry, the electrochemical behavior of complexes **3a-c** can involve a *quasi-reversible* reduction of titanium(IV) in the first two steps followed by two or three tetrapyrazinoporphyrazine-based reduction.

.

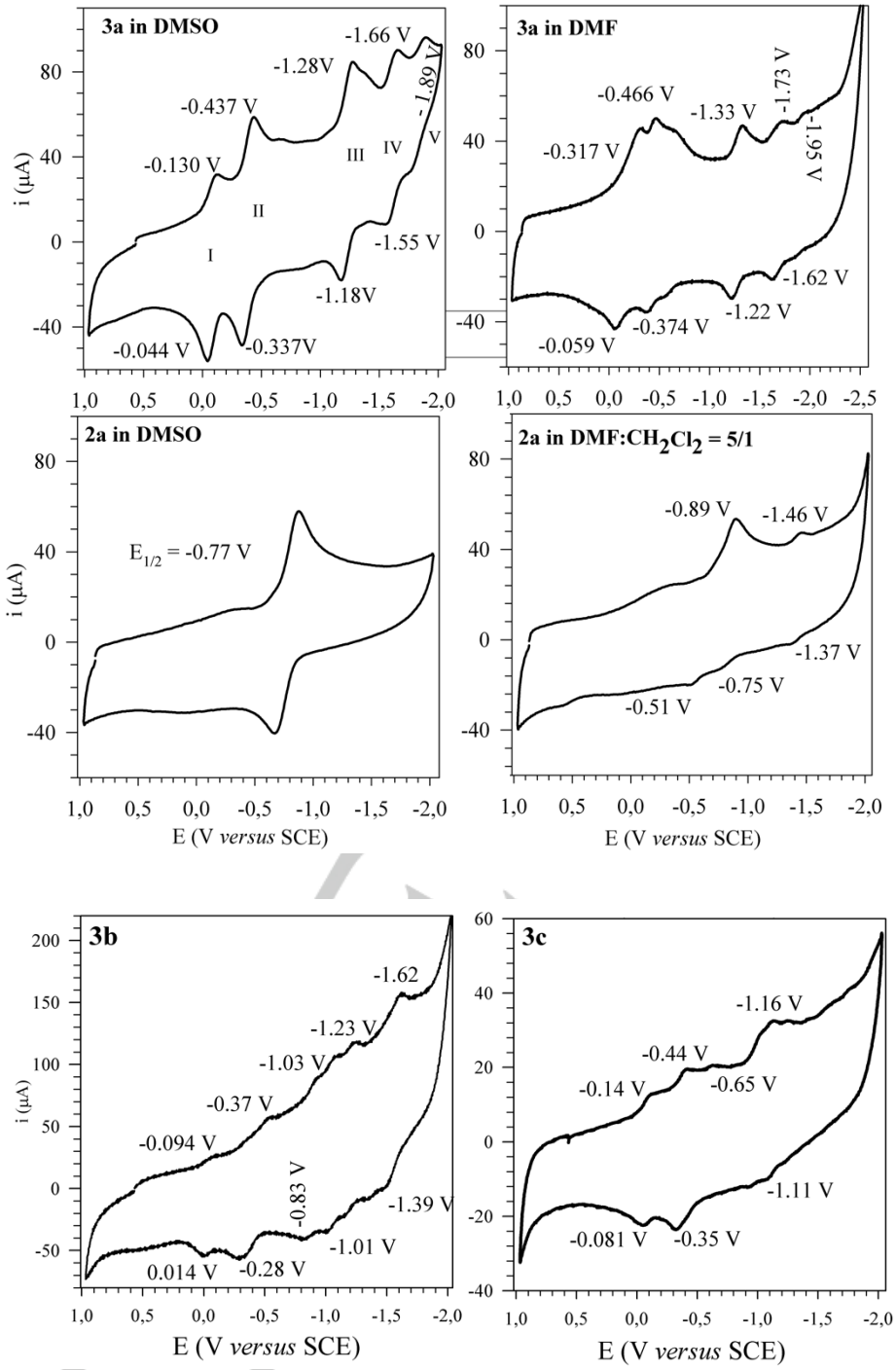

Figure 3. Top and middle: cyclic voltammograms of complex **3a** and ligand **2a** in DMSO and DMF, 0.1 M Bu_4NBF_4, scan rate 0.5 V/s. A mixture DMF/CH_2Cl_2 5/1 was applied as solvent in order to increase the solubility of ligand **2a**. Bottom: cyclic voltammograms of complex **3b** and **3c** in DMSO, 0.1 M Bu_4NBF_4, scan rate 0.5 V/s.

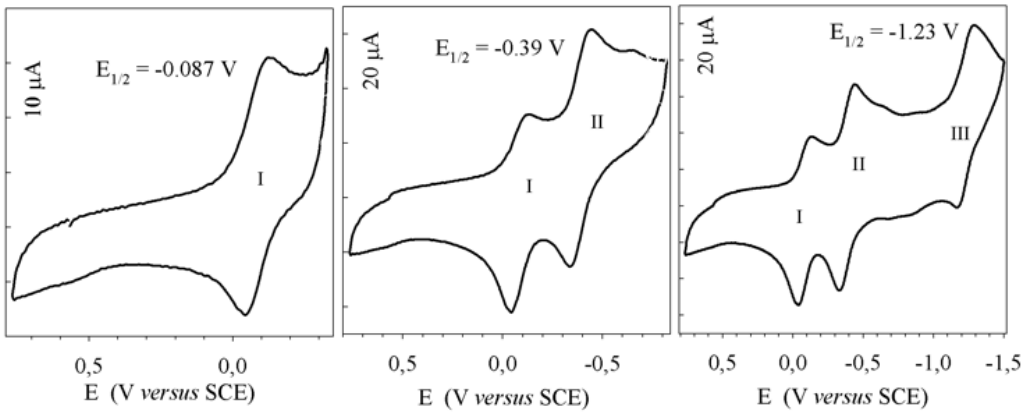

Figure 4. Cyclic voltammograms of complex **3a** in DMSO, 0.1 M Bu_4NBF_4, scan rate 0.5 V/s.

Table 2. Half-Wave Potentials[a] ($E_{1/2}$, V *vs* SCE) and potential separations between different stepwise reductions (Δ) of complexes **3a-c** and [**2b**-M^{II}]

Compound	I	II	III	IV	V	Δ_{I-II}	Δ_{II-III}	Δ_{III-IV}	Δ_{IV-V}
3a[b]	-0.087	-0.39	-1.23	-1.60	-1.89[c]	0.30	0.84	0.37	0.29
3a[c,d]	-0.32	-0.45	-1.33	-1.73	-1.95[c]	0.13	0.86	0.40	0.23
3b[b,c]	-0.062	-0.34	-1.00	-1.20	-1.58	0.28	0.66	0.20	0.38
3c[b,c]	-0.062	-0.39	-1.11			0.33	0.72		
[**2b**-Zn^{II}][e,f]	-0.34	-0.72	-1.38	-1.66	-1.83	0.38	0.66	0.28	0.17
[**2b**-Zn^{II}][f,g]	-0.26	-0.67	-1.38	-1.64		0.41	0.71	0.26	
[**2b**-Cu^{II}][f,g]	-0.22	-0.58	-1.22	-1.58		0.36	0.64	0.36	
[**2b**-Co^{II}][f,g]	-0.06	-0.76	-1.31	-1.77		0.70	0.55	0.46	
[**2b**-Mn^{II}][f,g]	-0.16	-0.89	-1.33	-1.64		0.73	0.44	0.47	
$(PhCH_2O)_4$Pc-$Ti^{IV}O$[h,i]	-0.18	-0.58	-1.51	-1.76		0.40	0.93	0.25	
$(PhOC_6H_4OCH_2)_4$Pc-$Ti^{IV}O$[h,i]	-0.14	-0.55	-1.42	-1.71		0.41	0.87	0.29	

[a]: $E_{1/2} = (E^p_c + E^p_a)/2$; [b]: DMSO, 0.1 M Bu_4NBF_4; scan rate 0.5 V/s; [c]: $E^p_{cathodic}$; [d]: DMF, 0.1 M Bu_4NBF_4; scan rate 0.5 V/s; [e] pyridine/0.1M TBAP, scan rate 0.1 V/s; [f]: ref [23]; [g]: DMF, 0.1M TBAP, scan rate 0.1 V/s; [h]: DMF, 0.1 M Bu_4NBF_4; scan rate 01 V/s; [i]: ref [24].

Cyclic voltammetry technique was also used to study the response of complex **3a** towards electrochemical processes, such as hydrogen and oxygen redox reactions, of practical interest in energy conversion devices. To improve the electronic conductivity of the sample, compound **3a** was blended with a carbon support (Vulcan XC72) in weight ratio 20:80 and mixed with 2-propanol and 5% Nafion solution in order to prepare the catalytst ink.[25] A catalyst ink based on Pt/C (E-TEK, with 20 wt.% Pt content with respect to C) was used as benchmark. A properly designed three electrode cell configuration was used to evaluate the catalytic activity of the sample: Ag/AgCl was used as reference electrode; a glassy carbon of 4 mm diameter disk, where a thin layer of catalyst ink was coated with a loading of 50 µg/cm^2 of the catalyst (**3a** or Pt) was adopted as the working electrode (WE). A platinum wire was used as counter electrode and the cell was filled with 0.1 M $HClO_4$ electrolyte.

Cyclic voltammetry was performed under nitrogen atmosphere with a scan rate of 50 mV/sec in the potential range 0,05 ÷ 1,2 V (all the potential values for this measurement were reported *versus* the reversible hydrogen electrode RHE).

Figure 5 shows the 50th voltammetric cycle recorded for both **3a**- and Pt-based samples. Interestingly, sample **3a** showed typical peaks due to hydrogen redox reactions (*i.e.* adsorption/desorption) visible at low potential, delivering higher current densities with respect to the Pt/C catalyst. Unfortunately, negligible electrochemical activity was observed at higher potential regions, where the oxygen reactions are expected.

This result could be explained considering the acidic properties of the sample sustained by the presence of the Ti-O system, which can participate in the hydrogen reactions by the reversible deprotonation equilibrium above explained (Scheme 2).

Furthermore, it is worth noticing pointing out that superior behavior has been obtained for bare **3a**/C composite toward hydrogen redox process with respect to platinum. The latter being the benchmark, commonly used catalyst for both hydrogen oxidation and evolution reactions occurring in a fuel cell or electrolyzer device, respectively.[26-27] Consequently, due to the intrinsic advantages of compound **3a** with respect to platinum, in terms of cost and scalability, the proposed Ti-based complex is considered of great interest, deserving further investigations to evaluate its applicability as catalytic material in fuel cell or water electrolyzer devices.

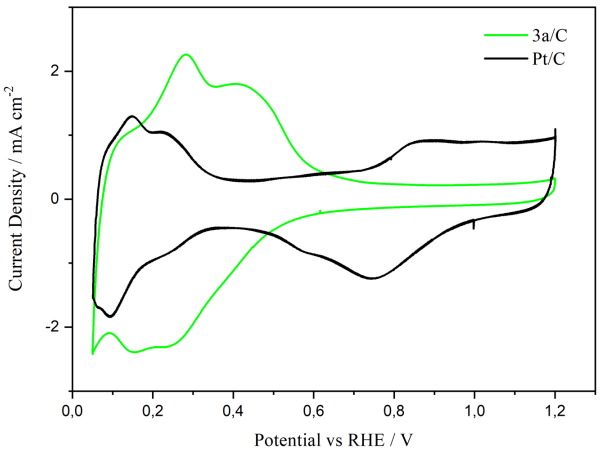

Figure 5. Cyclic voltammograms of the investigated **3a** sample (green) and of benchmark Pt/C (black) catalyst, analyzed in $HClO_4$, 0.1 M electrolyte at 50 mV/s scan rate.

IR Spectra.

Pyrazinoporphyrazine macrocycles object of this study exhibited quite similar IR spectral patterns. In general, signals of Ti-complexes were sharper and more intense than those of the corresponding ligands, especially between 900 and 1340 cm^{-1}. The porphyrazine macrocycle which is characterized by the presence of conjugated CC and CN double bonds, gave typical absorptions in the range 1000 – 1600 cm^{-1} due to skeletal vibrations.

Interestingly, the introduction of the Ti=O group in complexes **3a-c** caused the appearance of peaks located near 700 and 900 cm^{-1} (**3a**: 744 cm^{-1}, 906 cm^{-1}; **3b**: 704 cm^{-1}, 743 cm^{-1}, 993 cm^{-1}; **3c**: 762 cm^{-1}, 938 cm^{-1}).[10, 28-29] Because of the presence of the NH stretching, broad absorptions above 3000 cm^{-1} were observed for ligands **2b-c** (**2b**: 3292 cm^{-1}, **2c**: 3053 cm^{-1}), while for compound **2a** this broad peak was shifted to 2958 cm^{-1}. Complex **3c** also showed a broad absorption around 3056 cm^{-1}, which can be attributed to the stretching of aromatic CH (see Supporting Information for full IR spectra).

Solid State Studies:

Solid State NMR Studies.

For the characterization of all complexes, Solid State Nuclear Magnetic Resonance (SSNMR) ^{1}H-^{13}C Cross Polarization-Magic Angle Spinning (CP-MAS) spectra were acquired and compared with the spectra of the corresponding ligands. It should be noted that in CP spectra the relative intensities of the different peaks are not quantitative, since signals form carbon-13 nuclei in closest proximity to protons are enhanced by the cross-polarization process.

For complex **3a**, a single peak centered at 148.9 ppm was observed in the aromatic region, similarly to what already reported in literature [3], which is ascribable to carbons 1, 2 and 3 (Figure 6a). In the case of complex **3c**, three main peaks could be identified, which are centered at 128.4 ppm (carbons 5, 6, 7), 137.7 ppm (carbon 4) and at about 151.0 ppm (carbons 1, 2, 3) (Figure 6b). The spectrum of complex **3b** presented four main signals in the aromatic region centered at 123.7 ppm (carbons 5 and 7), 136.3 ppm (carbon 6), 147.9 ppm (carbon 8) and 155.6 ppm (carbons 1, 2, 3, 4) (Figure 6c). The spectra of all complexes and ligands also presented low intensity signals in the aliphatic region between 0 ppm and 70 ppm (Figure 6d-f), probably due to residual solvent molecules (such as acetone) co-crystallized with the complexes and/or to reaction by-products.

The spectra of each ligand presented carbon resonances similar to the ones observed for the corresponding complex; only a small change of their chemical shifts could be observed (ligand **2a**: 146.6 ppm; ligand **2b**:123.7 ppm, 136.9 ppm, 147.4 ppm, 155.1 ppm; ligand **2c**: 128.4 ppm, 137.2 ppm, 150.8 ppm; see Supporting Information), indicating that the coordination with the titanyl group induces only a slight modification of the symmetry and the conformational properties of the tetrapyrazinotetraazaporphyrine macrocycle.

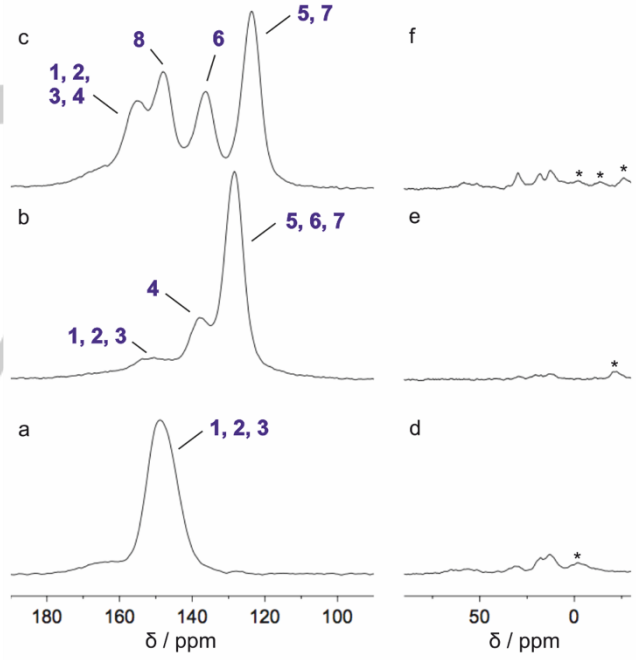

Figure 6. Aromatic (left panel) and aliphatic (right panel) regions of the ^{1}H-^{13}C CP-MAS spectra of complexes **3a** (a, d), **3c** (b, e) and R=**3b** (c, f). Spinning side bands are marked with asterisks.

MALDI-TOF Analysis.

Ligands and complexes were further analyzed by MALDI-TOF analysis employing 2,5-dihydroxybenzoic acid (DHB) as matrix. DHB was preferred because it undergoes less fragmentation respect to other reference compounds under laser shot (data not shown). To this end, samples were prepared according to the procedures reported in the following references.[30-32] In general, for ligands **2a-c**, the precursor ion results from the addition of a proton to form the positively charged molecular ion $[M+H]^{+}$ (see

Supporting Information for related measurements). Moreover, sodium $[M+H+Na]^+$ and potassium $[M+H+K]^+$ adducts were also identified. Similarly, complexes **3a-c** were detected as precursor ion $[M+H]^+$ as well as in cation adduct clusters. MALDI spectra and a summary of all the ligands and complexes species detected are displayed in Supplemental Information.

Morphological Studies by SEM.

Morphological studies of all Titanium-based complexes were carried by SEM analysis, as shown in Figure 6. Among all samples, material **3a** displayed unique morphological features, resulting in agglomerates of quasi-spherical particles with spotty flat mats. When the complexity of the molecule structure increases, *i.e.* with the introduction of eight 2-pyridil and eight phenyl groups (samples **3b** and **3c** respectively), the corresponding particles exhibit important changes in terms of both shape and size distributions, as more homogeneous, layered-like structures were observed.

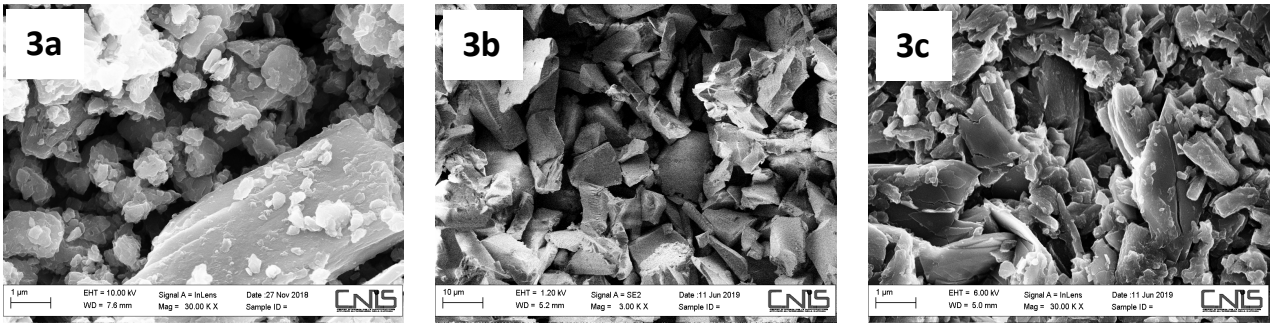

Figure 6. SEM images of all Titanium-based complexes.

Conclusion

In summary, this paper presented the synthesis, characterization and the electrochemical behavior of a family of ligands and Ti-complexes based on the tetrakis-2,3-[5,6-di-R_8-pyrazino]porphyrazine (R= H, 2-Py, Ph) macrocycle. Ligands **2a-c** were obtained by cyclotetramerization of precursors **1a-c** in the presence of DBU as catalyst, while complexes **3a-c** could be prepared by precursors melting and addition of Titanium(IV) butoxide under inert gas and dry reaction conditions. Molecular aggregation was confirmed by UV-Vis studies in different solvents. IR spectra were characterized by typical absorptions due to CC and CN skeletal vibrations. Complexes showed additional peaks related to the Ti=O group in the range 700 - 900 cm^{-1}. Broad bands due to NH stretching were also observed for the ligands. MALDI-TOF analysis was performed in order to further investigate the structures. $[M+H]^+$ adducts as well cation adduct clusters were identified for both compounds **2a-c** and **3a-c**. Morphological studies by SEM revealed a change in the morphological features with an increase in homogeneity passing from **3a** to **3b-c**. The electrochemical characterization was carried out in DMSO/Bu_4NBF_4 0.1 M. In general, ligands showed only one reversible peak that can be attributed to the dianion reduction. Despite the low solubility, it was possible to observe different redox events of low intensity for compounds **3b-c**, while complex **3a** gave well defined voltammograms. From the results obtained, we proposed that our Ti-complexes can participate in up to five redox events. The first two involving the step-wise *quasi-reversible* reduction of the metal centre ($Ti^{IV} \rightarrow Ti^{III}$ and $Ti^{III} \rightarrow Ti^{II}$), while the remaining two or three reductions occur on charge of the TPysPz macrocycle. In the light of a future application of compounds **3a-c** in energy conversion devices, such as fuel cell or water electrolyzer, we realized a preliminary study to test the response of these catalysts towards hydrogen and oxygen redox reactions. Therefore, an ink of catalyst blended on a carbon support was used to coat **3a** on a glassy carbon. No activity toward oxygen redaction was observed but, interestingly, the presence of the Ti-O system confers the catalyst the ability to participate in hydrogen reactions delivering higher current densities with respect to Pt/C, introducing this catalyst as a possible alternative to Pt. Evaluation of the applicability of these materials as catalysts in energy conversion devices is ongoing.

Experimental Section

General

Analytical grade solvents and all commercially available reagents were used as received. Reactions were monitored by thin-layer chromatography using silica gel plates TLC Silica gel 60 F254 from Sigma-Aldrich; visualization was accomplished with UV light (254 nm) or $KMnO_4$ stain. Flash chromatography (FC) was carried out using Merck silica gel 60 (230-400 mesh) employing mixtures of petroleum ether and acetone as eluant. ^{1}H-NMR spectra of starting materials were recorded on a Bruker Avance 300 spectrometer (^{1}H: 300 MHz at 295 K). Chemical shifts were reported to the solvent residual peak (CDCl3: ^{1}H = 7.26 ppm). SSNMR spectra of all complexes and their respective ligands were acquired on a Varian

InfinityPlus spectrometer working at a Larmor frequency of 400.34 and 100.67 MHz for ^{1}H and ^{13}C, respectively, using a CP-MAS 3.2 mm probe. ^{1}H-^{13}C CP-MAS spectra were recorded using a contact time of 2 ms, under High-Power Decoupling from ^{1}H nuclei, at a MAS frequency of 15 kHz. 15000-80000 transients were accumulated, using a recycle delay of 3 s between consecutive transients. ^{13}C chemical shifts were referred to hexamethylbenzene and TMS as secondary and primary references, respectively. UV-vis spectra were recorded with a Hewlett Packard 8452 diode array spectrophotometer equipped with an external water bath circulator (Julabo Labortechnik, GmbH) for temperature control (± 0.1 °C), using quartz cuvettes with 1 cm optical path. ATR FT-IR spectra were recorded using a Thermo Scientific Nicolet iS10 spectrometer equipped with a triglycine sulfate detector (DTGS) and acquired with Omnic vers. 8.1.10 software. The spectra were the result of 32 scans with a spectral resolution of 4 cm^{-1}. An ATR correction algorithm and automatic atmospheric suppression were applied to all spectra. Cyclic voltammetry was performed on a homemade electrochemical equipment consisting of a computer-controlled potentiostat with Vernier Software Multi Purpose Laboratory Interface (MPLI) program for Windows, a glassy-carbon disk (diameter of 1 mm) as working electrode; an Ag/AgCl/KCl 3 M as the reference electrode (E *vs* SCE = E *vs* Ag/AgCl -0.032), and a platinum disc (surface 1 cm^2) as the auxiliary electrode. Cyclic voltammograms were acquired at 0.5 V/sec scan speed, 25°C, in DMF or DMSO containing Bu_4NBF_4 (0.1M) as supporting electrolyte. Concentration of ligands or complexes was 2 mM. Mass Spectrometry Analysis MALDI-TOF-MS spectra were acquired using a 5800 MALDI TOF/TOF Analyzer (Sciex, Ontario, Canada). The spectra were acquired in the positive reflector mode by 20 subspectral accumulations (each consisting of 50 laser shots) in an 50−1500 mass range, focus mass 800 Da, using a 355 nm Nb:YAG laser with a 20 kV acceleration voltage. Peak labelling was automatically done by 4000 Series Explorer software Version 4.1.0 (Sciex) without any kind of smoothing of peaks or baseline, considering only peaks that exceeded a signal-to noise ratio of 10 (local noise window 200 m/z) and a half maximal width of 2.9 bins. Calibration was performed using default calibration originated by five standard spots. 2,5-dihydroxybenzoic acid (DHB) was employed as matrix. SEM images were obtained from AURIGA Zeiss Field Emission.

Synthesis of starting materials 1a-c: Compounds **1a**-**c** were obtained by a modification of the procedure reported in ref. [17]. A solution of diaminomaleonitrile (18.5 mmols; 1 Equiv.) and the corresponding α-diketone (20.4 mmols; 1.1 Equiv.) in glacial acetic acid (35 mL) was heated under reflux for 3 hours. When the diaminomaleonitrile was totally consumed, the reaction mixture was cooled down and 50 mL of water were added. The aqueous layer was extracted with 100 mL of ethyl acetate and then washed according to the following sequence with water (3 x 50 mL), a saturated solution of $NaHCO_3$ (4 x 50 mL; exothermic reaction), water (2 x 50 mL) and brine (2 x 50 mL). The organic layer was dried over sodium sulfate. After filtration, the solvent was removed under reduced pressure and the solid residue was purified by recrystallization from ethanol/water at 4°C.

1a: m.p. 180°C; ^{1}H NMR (300 MHz, $CDCl_3$): δ= 8.94 (s, 2 H); 76% yield.

1b: m.p. 175°C; ^{1}H NMR (300 MHz, $CDCl_3$): δ= 8.31 ppm (d, J= 6 Hz, 1H), 8.06 ppm (d, J= 9 Hz, 1H), 7.96-7.84 (m, 1H), 7.40-7.28 (m, 1H); 73% yield.

1c: m.p. 240°C; ^{1}H NMR (300 MHz, DMSO-d_6): δ= 7.58-7.45 (m, 3H), 7.45-7.33 (m, 2H); 85% yield.

Synthesis of ligands 2a-c: Pyrazinoporphyrazine macrocycles **2a**-**c** were prepared by autocyclotetramerization of starting materials **1a**-**c** as follows: the precursor (400 mg; 3.1 mmols) was placed in a thick test tube and heated in an oil or sand bath until the solid melted (temperature of oil/sand bath employed: compound **1a**: 180°C; compound **1b**: 175°C; compound **1c**: 240°C). A few drops of DBU were added as catalyst. The mixture was manually stirred until a black solid was formed. After complete solidification, the solid was cooled down, finely grounded and purified by Soxhlet extraction with methanol (16 h) followed by acetone (10 h). The green or bluish powders were dried under vacuum until they reach a constant weight

2a: ^{13}C (SSNMR): 146.6 ppm. FTIR-ATR: $\tilde{\nu}$= 722, 725, 857, 890, 1150, 1118, 1193, 1356, 1429, 1599, 1868, 2111, 2936 cm^{-1}; UV/Vis (DMF): λ= 636, 576, 435, 404 nm; MS (MALDI-TOF): *m/z* calc for $C_{24}H_{11}N_{16}$: 523,1353 $[M+H]^+$; found 523.0859; *m/z* calc for $C_{24}H_{11}N_{16}Na$: 546.1250 $[M+H+Na]^{2+}$; found 546.2062. Elemental analysis calc for **2a·2C$_2$H$_6$O**: C 56.43%, H 3.47%, N 35.08%. Found: C 56.67%, H 3.42%, N 35.66%; 21% yield.

2b: ^{13}C (SSNMR): 123.7 ppm, 136.9 ppm, 147.4 ppm, 155.1 ppm. FTIR-ATR: $\tilde{\nu}$= 648, 696, 744, 759, 801, 950, 992, 1092, 1105, 1144, 1225, 1360, 1431, 1470, 1500, 1585, 1566, 1864, 2096, 3285 cm^{-1}; UV/Vis (DCM): λ= 668, 634, 617, 605, 581, 421, 355 nm; MS (MALDI-TOF): *m/z* calc for $C_{64}H_{35}N_{24}$: 1140.3229 $[M+H]^+$; found 1139.3477; *m/z* calc for $C_{64}H_{35}N_{24}Na$: 1162.3374 $[M+H+Na]^{2+}$; found 1162.3042. Elemental analysis calc for **2b·2H$_2$O**: C 65.42%, H 3.26%, N 28.60%. Found: C 65.13%, H 3.56%, N 27.44%; 20% yield.

2c: ^{13}C (SSNMR): 128.4 ppm, 137.2 ppm, 150.8 ppm. FTIR-ATR: $\tilde{\nu}$= 689, 765, 1023, 1173, 1340, 1523, 1860, 2103, 3053 cm^{-1}; UV/Vis (DMF): λ= 657, 336 nm; UV/Vis (DCM): λ= 667, 638, 342 nm; MS (MALDI-TOF): *m/z* calc for $C_{72}H_{43}N_{16}$: 1131.3857 $[M+H]^+$; found 1131.2971; *m/z* calc for $C_{72}H_{43}N_{16}Na$: 1154.3754 $[M+H+Na]^{2+}$; found 1154.2932. Elemental analysis calc for **2c**: C 76.45%, H 3.74%, N 19.80%. Found: C 77.27%, H 4.04%, N 18.36%; 18% yield.

Synthesis of complexes 3a-c: Titanium-based pyrazinoporphyrazines **3a**-**c** were prepared by cyclotetramerization of starting materials **1a**-**c** in the presence of titanium (IV) butoxide as follows: the precursor **1a**-**c** (400 mg; 3.1 mmols; 8 Equiv.) was placed under argon in a dry Schlenk flask and heated in an oil or sand bath until the solid melted (temperature of oil/sand bath employed: compound **1a**: 180°C; compound **1b**: 175°C; compound **1c**: 240°C). Against a flux of inert gas, titanium (IV) butoxide (0.39 mmols; 1 Equiv.) was added. The evolution of a white smoke was generally observed. The reaction mixture was stirred at high temperature (temperature of oil/sand bath employed: starting-material **1a**: 180°C; starting-material **1b**: 175°C; starting-material **1c**: 240°C) for 5 hours, then the mixture was cooled down, 30 mL of MeOH were added and the crude product was left under stirring overnight. The solid obtained was separated by centrifugation and brought to constant weight under vacuum. In order to dissolve the contaminants, the complex **3a**-**c** finely grounded, were then resuspended in CH_2Cl_2 and left under stirring for 30 minutes. After this time, the product **3a**-**c** was collected by centrifugation and dried under vacuum until constant weight

3a: ^{13}C (SSNMR): 148.9 ppm. FTIR-ATR: $\tilde{\nu}$= 744, 906, 909, 913, 1208, 1359, 1507, 1508, 1664, 1864, 2110 cm^{-1}; UV/Vis (DMF): λ= 647, 587, 326 nm; UV/Vis (DCM): λ= 646, 614, 585, 338 nm; MS (MALDI-TOF): *m/z* calc for $C_{24}H_9N_{16}OTi$: 585.0625 $[M+H]^+$; found 584.9780. Elemental analysis calc for **3a·2H$_2$O**: C 46.47%, H 1.95%, N 36.12%. Found: C 46.23%, H 3.03%, N 33.03%; blue powder obtained with 78% yield.

3b: ^{13}C (SSNMR): 123.7 ppm, 136.3, 147.9, 155.6 ppm. FTIR-ATR: $\tilde{\nu}$= 705, 744, 790, 958, 993, 1092, 1147, 1359, 1432, 1471, 1566, 1584, 1738, 2113 cm^{-1}; UV/Vis (DMF): λ= 667, 603, 315 nm; UV/Vis (DCM): λ= 668, 634, 605, 577, 320 nm; MS (MALDI-TOF): *m/z* calc for $C_{64}H_{33}N_{24}NaOTi$: 1224.2646 $[M+H+Na]^{2+}$; found 1224.3872; Elemental analysis calc for **3b·6H$_2$O**: C 58.73%, H 3.39%, N 25.67%. Found: C 58.43%, H 4.06%, N 24.19%; green powder obtained with 65% yield.

3c: ^{13}C (SSNMR): 128.4 ppm, 137.7 ppm, 151.0 ppm. FTIR-ATR: $\tilde{\nu}$= 690, 768, 938, 1024, 1104, 1143, 1180, 1231, 1341, 1444, 1540, 1631, 1885, 2102, 3051, 3288 cm^{-1}; UV/Vis (DMF): λ= 665, 601, 375 nm; UV/Vis (DCM): λ= 666, 637, 607, 445, 362 nm; MS (MALDI-TOF): *m/z* calc for $C_{72}H_{41}N_{16}OTi$: 1193.3129 $[M+H]^+$; found 1193.2933; Elemental analysis

calc for **3c·2H₂O**: C 70.36%, H 3.61%, N 18.23%. Found: C 70.05%, H 3.88%, N 17.47%; green powder obtained with 95% yield.

Acknowledgements

P.R. and L.M. thanks University of Rome La Sapienza (Progetto per Avvio alla Ricerca-Tipo 2, AR218164173B286E; and Progetto per Avvio alla Ricerca-Tipo 1, AR118164309CF528, respectively) and Prof. Stefania Panero for the financial support and fruitful discussion.

Keywords: Tetrapyrazinoporphyrazine • Titanium complex • Electrochemical Behavior • Spectroscopic Properties

[1] V. Novakova, M. P. Donzello, C. Ercolani, P. Zimcik, P. A. Stuzhin, *Coord. Chem. Rev.* **2018**, *361*, 1-73.
[2] M. P. Donzello, C. Ercolani, V. Novakova, P. Zimcik, P. A. Stuzhin, *Coord. Chem. Rev.* **2016**, *309*, 107-179.
[3] D. Dini, M. Hanack, H.-J. Egelhaaf, J. C. Sancho-García, J. Cornil, *J. Phys. Chem. B* **2005**, 1*09*, 5425-5432.
[4] M. Saxena, S. A. Loza-Rosas, K. Kavita Gaur, S. Sharma, S. C. Pérez Otero, A. D. Tinoco, *Coord. Chem. Rev.* **2018**, *363*, 109-125;
[5] M. A. Tarselli, *Nat. Chem.* **2013**, *5*, 546.
[6] R. Guilard, J.-M. Latour, C. Lecomte, J.-C. Marchon, J. Protas, D. Ripoll, *Inorg. Chem.* **1978**, *17*, 1228-1237.
[7] M. F. Sisemore, M. Selke, J. N. Burstyn, J. Selverstone Valentine *Inorg. Chem.* **1997**, *36*, 979-984.
[8] W.-L. Hea, F. Fanga, D.-M. Maa, M. Chena, D.-J. Qiana, M. Liu, *Appl. Surf. Sci.* **2018**, *427*, 1003-1010.
[9] M. Mayukh, C. M. Sema, J. M. Roberts, D. V. McGrath, *J. Org. Chem.* **2010**, *75*, 7893–7896.
[10] M. A. Faraonov, D. V. Konarev, A. M. Fatalov, S. S. Khasanov, S. I. Troyanov, R. N. Lyubovskaya, *Dalton Trans* **2017**, *46*, 3547-3555.
[11] W. Zhang, L. Wenzhen, R. Cao, *Chem. Rev.* **2017**, *117*, 3717−3797.
[12] J. M. Luque-Centeno, M. V. Martínez-Huerta, D. Sebastián, G. Lemes, E. Pastor, M. J. Lázaro, *Renewable Energy* **2018**, *125*, 182-192.
[13] G. Lovat, D. Forrer, M. Abadia, M. Dominguez, M. Casarin, C. Rogero, A. Vittadini, L. Floreano, *J. Phys. Chem. C* **2017**, *121*, 25, 13738-13746.
[14] V. G. Rao, B. Dhital, Y. He, H. P. Lu, *J. Phys. Chem. C* **2014**, *118*, 35, 20209-20221.
[15] A. F. Nogueira, L. F. O. Furtado, A. L. B. Formiga, M. Nakamura, K. Araki, H. E. Toma, *Inorg. Chem.* **2004**, *43*, 2, 396-398.
[16] T. Matsumoto, K. Takamura, *Anal. Methods* **2012**, *4*, 4289-4294.
[17] E. H. Mørkved, H. Ossletten, H. Kjøsen, O. Bjørlo, *J. Prakt. Chem.* **2000**, *342*, 83-86.
[18] M. P. Donzello, Z. Ou, F. Monacelli, G. Ricciardi, C. Rizzoli, C. Ercolani, K. M. Kadish, *Inorg. Chem.* **2004**, *43*, 8626-8636.
[19] M. P. Donzello, Z. Ou, D. Dini,M. Meneghetti, C. Ercolani, K. M. Kadish, *Inorg. Chem.* **2004**, *43*, 8637-8648.
[20] A. R. Monahan, J. A. Brado, A. F. DeLuca, A. F. *J. Phys. Chem*. **1972**,*76*, 1994-1996.
[21] P. A. Stuzhin, A. S. Malyasova, V.B. Sheinin, E. Kokareva, P. A. Tarakanov, O. I. Koifman, *Dyes Pgm*, **2017**, *139*, 509-516;
[22] M. Pişkin, N. Öztürk, M. Durmuş, *J. Mol. Struct.* **2017**, *1149,* 893-899.
[23] C. Bergami, M. P. Donzello, F. Monacelli, C. Ercolani, K. M. Kadish, *Inorg. Chem.,* **2005**, *44*, 9862-9873.
[24] P. Tau, T. Nyokong, *Electrochim. Acta* **2007**, *52*, 3641-3650.
[25] L. Mazzapioda, C. Lo Vecchio, A. Paolone, A. S. Aricò, V. Baglio, M. A. Navarra, *Chem. Electro. Chem*, **2019**, *6*, 5941-5945.
[26] L. Mazzapioda, S. Panero, M. A. Navarra, *Polymers* **2019**, *11*, 914-923.
[27] S. Siracusano, V. Baglio, I. Nicotera, L. Mazzapioda, A. S. Aricò, S. Panero, M. A. Navarra, *Int. J. Hydrogen Energy* **2017**, *42*, 27851-27858.
[28] H. Fujii, T. Kurahashi, T. Tosha, T. Yoshimura, T. Kitagawa, *J.Inorg. Biochem.* **2006**, *100*, 533–541.
[29] D. K. Tarakci, I. Gürol, V. Ahsen, *J. Porphyrins Phthalocyanines* **2013**, *17*, 548–554.
[30] D. M. Mayukh, C. M. Sema, J. M. Roberts, D. V. McGrath, *J. Org. Chem.* **2010**, *75*, 7893–789.
[31] R. Lidgard, M. W. Duncan, *Rapid Commun. Mass Sp.* **1995**, *9*, 128-132.
[32] M. Canlica, T. Nyokong, *Polyedron* **2011**, *30*, 1975-1981.

Entry for the Table of Contents

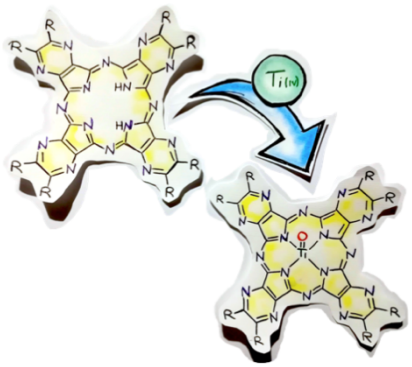

Tetrapyrazinoporphyrazines are privileged frameworks present in ligands and metal complexes. Choosing titanium as metal center, herein, we unveil the synthesis, the characterization and the electrochemical behavior of tetrakis-2,3-[5,6-di-R_8-pyrazino]porphyrazine (R= H, 2-Py, Ph) ligands and Ti-complexes.

Supplemental Material for:

Titanium-based tetrakis-2,3-[5,6-di(substituted)pyrazino]porphyrazine: synthesis and characterization

Table of contents

1. Materials and Methods

Analytical grade solvents and all commercially available reagents were used as received.
Reactions were monitored by thin-layer chromatography using silica gel plates TLC Silica gel 60 F254 from Sigma-Aldrich; visualization was accomplished with UV light (254 nm) or $KMnO_4$ stain. Flash chromatography (FC) was carried out using Merck silica gel 60 (230-400 mesh) employing mixtures of petroleum ether and acetone as eluant.
UV-vis spectra were recorded with a Hewlett Packard 8452 diode array spectrophotometer equipped with an external water bath circulator (Julabo Labortechnik, GmbH) for temperature control (± 0.1 °C), using quartz cuvettes with 1 cm optical path.
^{1}H-NMR spectra of starting materials were recorded on a Bruker Avance 300 spectrometer (^{1}H: 300 MHz at 295 K). Chemical shifts were reported to the solvent residual peak (CDCl3: ^{1}H = 7.26 ppm).
SSNMR spectra of all complexes and their respective ligands and were acquired on a Varian InfinityPlus spectrometer working at a Larmor frequency of 400.34 and 100.67 MHz for ^{1}H and ^{13}C, respectively, using a CP-MAS 3.2 mm probe. ^{1}H-^{13}C CP-MAS spectra were recorded using a contact time of 2 ms, under High-Power Decoupling from ^{1}H nuclei, at a MAS frequency of 15 kHz. 15000-80000 transients were accumulated, using a recycle delay of 3 s between consecutive transients. ^{13}C chemical shifts were referred to hexamethylbenzene and TMS as secondary and primary references, respectively.
Cyclic voltammetry was performed on a homemade electrochemical equipment consisting of a computer-controlled potentiostat with Vernier Software Multi Purpose Laboratory Interface (MPLI) program for Windows, a glassy-carbon disk (diameter of 1 mm) as working electrode; an Ag/AgCl/KCl 3 M as the reference electrode (E *vs* SCE = E *vs* Ag/AgCl -0.032), and a platinum disc (surface 1 cm^2) as the auxiliary electrode (Friis, E. P.; Andersen, J. E. T.; Madsen, L. L.; Bonander, N.; Moller, P.; Ulstrup, J. *Electrochimica Acta* **199**8, *43*, 1114). Cyclic voltammograms were acquired at 0.5 V/sec scan speed, 25°C, in DMF or DMSO containing Bu_4NBF_4 (0.1M) as supporting electrolyte. Concentration of ligands or complexes was 2 mM.
ATR FT-IR spectra were recorded using a Thermo Scientific Nicolet iS10 spectrometer equipped with a triglycine sulfate detector (DTGS), and acquired with Omnic vers. 8.1.10 software. The spectra were the result of 32 scans with a spectral resolution of 4 cm^{-1}. A Smart iTR ATR accessory provided with a diamond ATR crystal was used. An ATR correction algorithm and automatic atmospheric suppression were applied to all spectra.
Mass Spectrometry Analysis MALDI-TOF-MS spectra were acquired using a 5800 MALDI TOF/TOF Analyzer (Sciex, Ontario, Canada). The spectra were acquired in the positive reflector mode by 20 subspectral accumulations (each consisting of 50 laser shots) in an 50−1500 mass range, focus mass 800 Da, using a 355 nm Nb:YAG laser with a 20 kV acceleration voltage. Peak labelling was automatically done by 4000 Series Explorer software Version 4.1.0 (Sciex) without any kind of smoothing of peaks or baseline, considering only peaks that exceeded a signal-to noise ratio of 10 (local noise window 200 m/z) and a half maximal width of 2.9 bins. Calibration was performed using default calibration originated by five standard spots (Mass Standards kit for Calibration P/N 4333604). 2,5-dihydroxybenzoic acid (DHB) was employed as matrix.
Scanning electron microscopy (SEM) analysis was performed using an AURIGA Zeiss Field Emission.

2. General procedures and characterization

2.1 *General procedure for the preparation of starting material **1a-c***

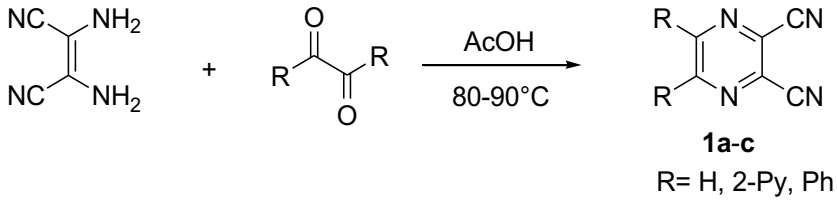

Compounds **1a-c** were obtained by a modification of the procedure reported by Mørkved *et al.* (Mørkved, E. H.; Ossletten, H.; Kjøsen, H.; Bjørlo, O. *J. Prakt. Chem.* **2000**, *342*, 83).
A solution of diaminomaleonitrile (18.5 mmols; 1 Equiv.) and the corresponding α-diketone (20.4 mmols; 1.1 Equiv.) in glacial acetic acid (35 mL) was heated under reflux for 3 hours. When the diaminomaleonitrile was totally consumed, the reaction mixture was cooled down and 50 mL of water were added. The aqueous layer was extracted with 100 mL of ethyl acetate and then washed according to the following sequence with water (3 x 50 mL), a saturated solution of $NaHCO_3$ (4 x 50 mL; exothermic reaction), water (2 x 50 mL) and brine (2 x 50 mL). The organic phase was dried over sodium sulfate. After filtration, the solvent was removed under reduced pressure and the solid residue was purified by recrystallization from ethanol/water at 4°C. Products were obtained with the following yields: compound **1a** 76% yield; compound **1b** 73% yield; compound **1c** 85% yield.

2.2 *Characterization of starting materials **1a-c***

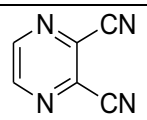 **1a**	**1a**. **^{1}H-NMR** (300 MHz, $CDCl_3$): 8.94 ppm (s, 2 H).
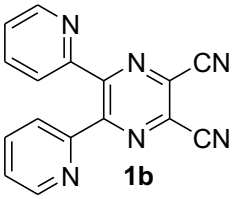 **1b**	**1b**. **^{1}H-NMR** (300 MHz, $CDCl_3$): 8.31 ppm (d, 1H; J= 6 Hz); 8.06 ppm (d, 1H; J= 9 Hz); 7.96-7.84 (m, 1H); 7.40-7.28 (m, 1H).
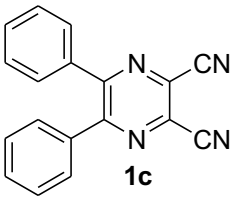 **1c**	**1c**. **^{1}H-NMR** (300 MHz, DMSO-d_6): 7.58-7.45 (m, 3H); 7.45-7.33 (m, 2H).

*2.3 [1]H-NMR spectra of starting materials **1a-c***

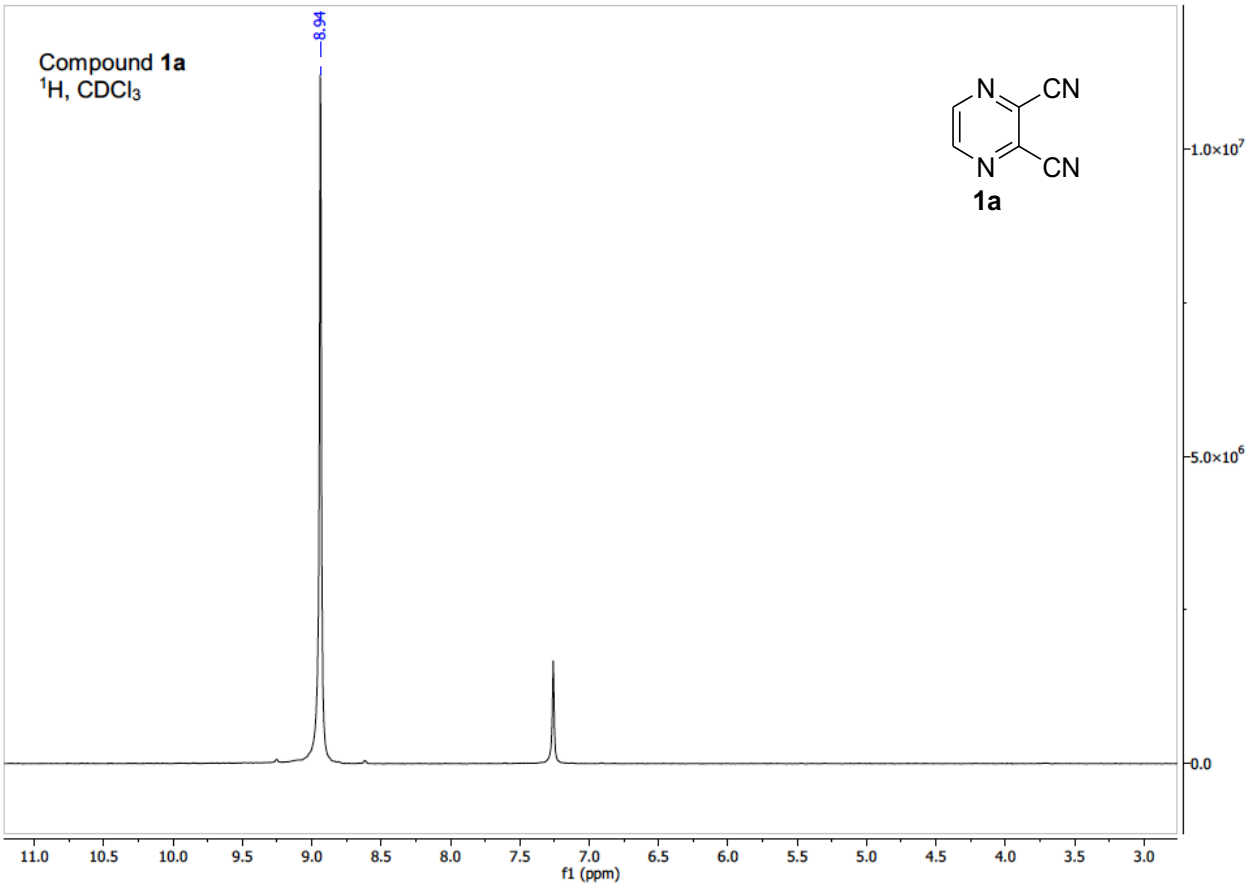

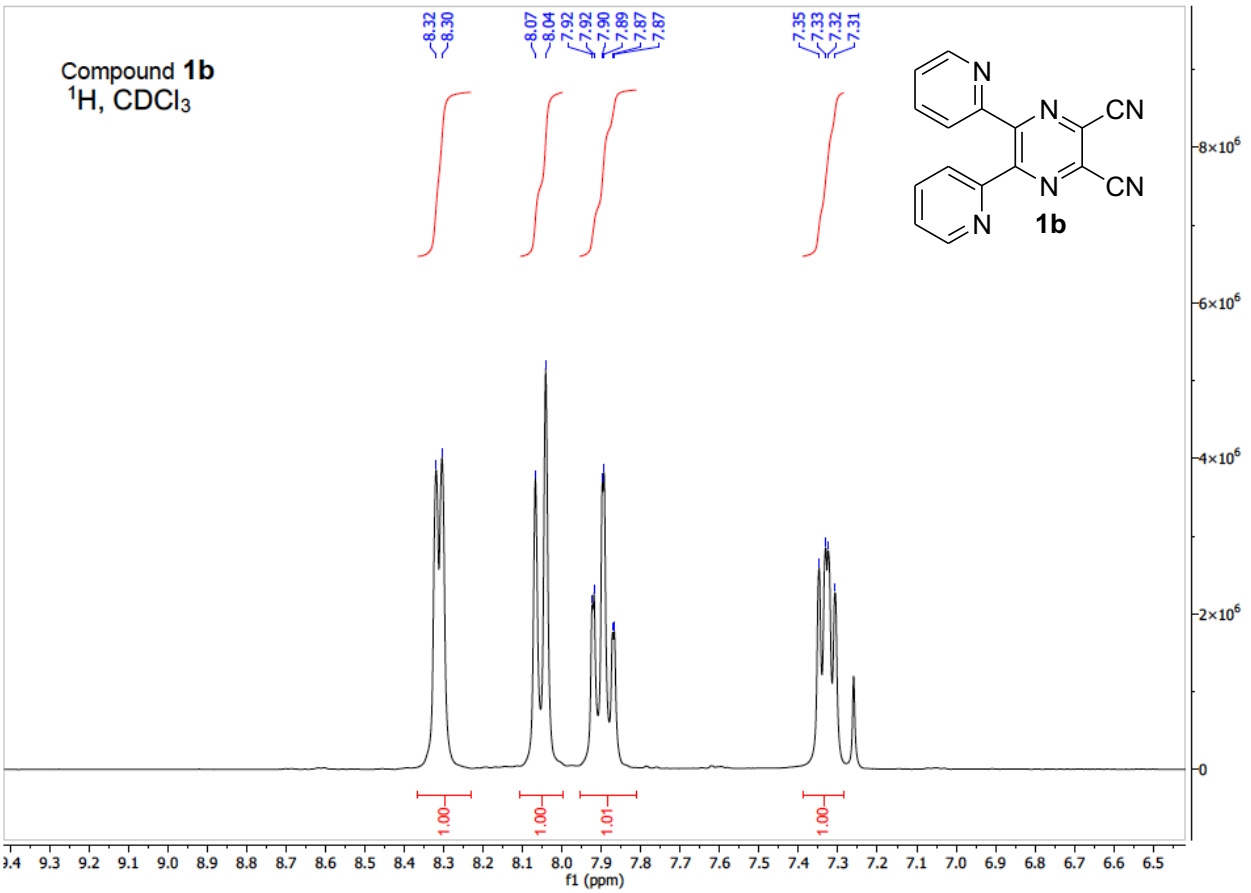

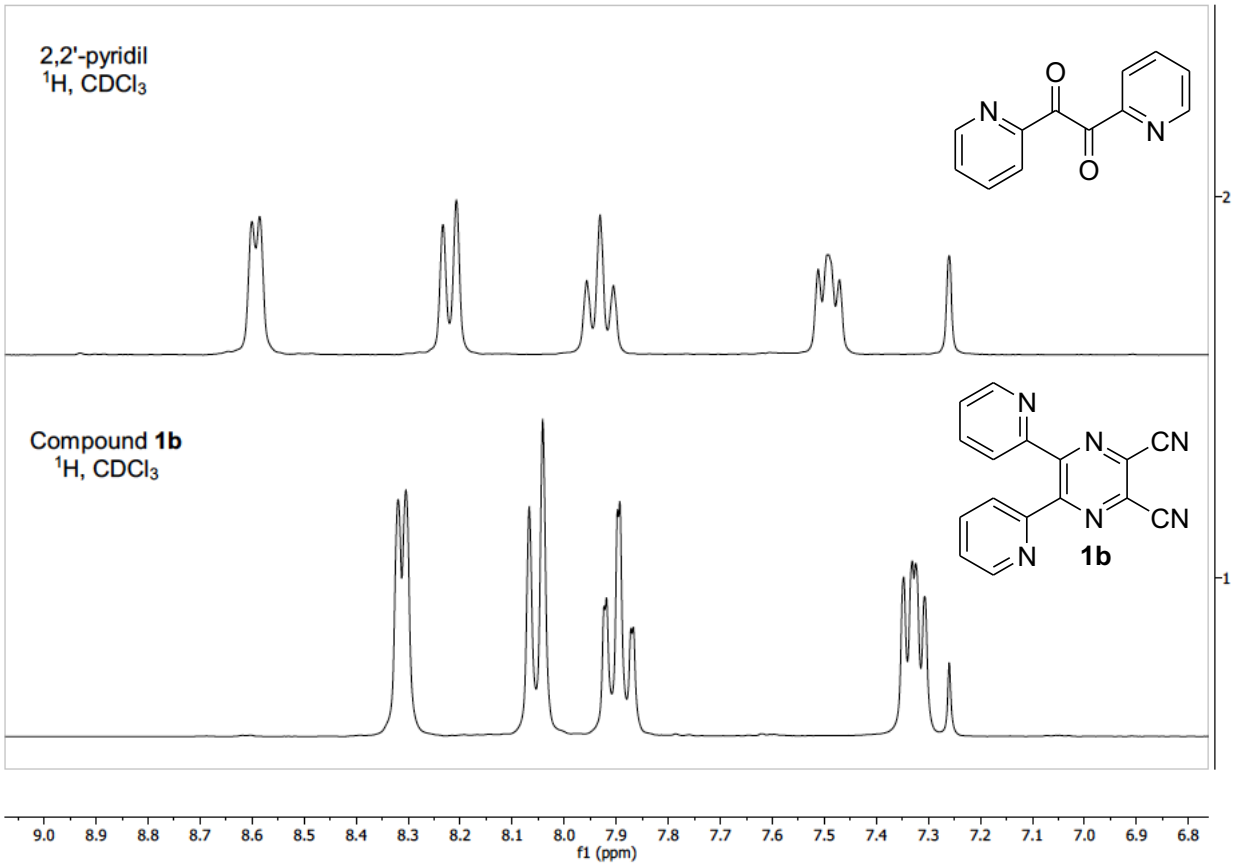
2,2'-pyridil
^{1}H, CDCl$_3$
O
O
N
N
Compound **1b**
^{1}H, CDCl$_3$
N
N
CN
N
CN
N
1b
2
1
9.0 8.9 8.8 8.7 8.6 8.5 8.4 8.3 8.2 8.1 8.0 7.9 7.8 7.7 7.6 7.5 7.4 7.3 7.2 7.1 7.0 6.9 6.8
f1 (ppm)

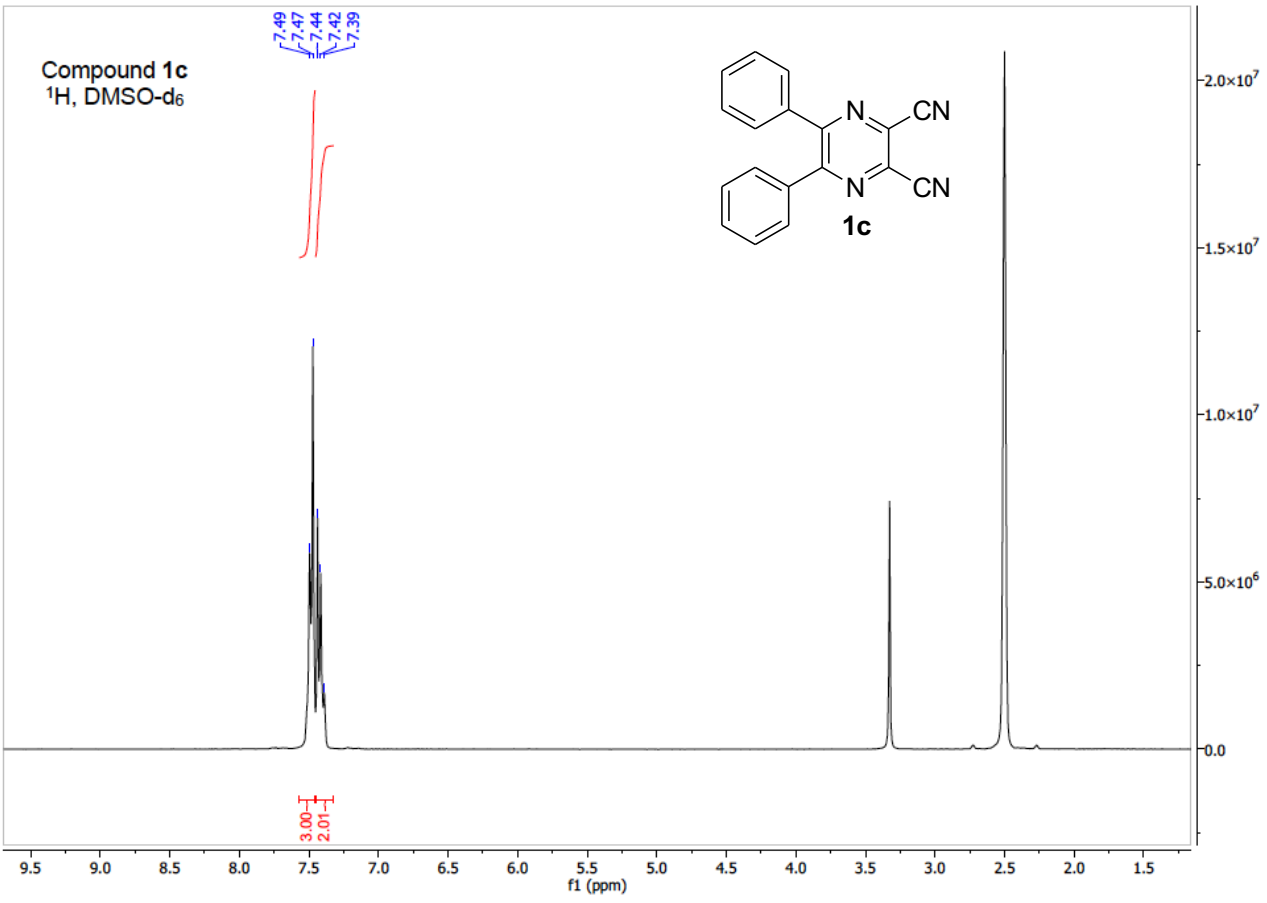
Compound **1c**
^{1}H, DMSO-d$_6$
7.49
7.47
7.44
7.42
7.39
N
CN
N
CN
1c
3.00
2.01
2.0×10^7
1.5×10^7
1.0×10^7
5.0×10^6
0.0
9.5 9.0 8.5 8.0 7.5 7.0 6.5 6.0 5.5 5.0 4.5 4.0 3.5 3.0 2.5 2.0 1.5
f1 (ppm)

2.4 *General procedure for the preparation of ligands **2a-c***

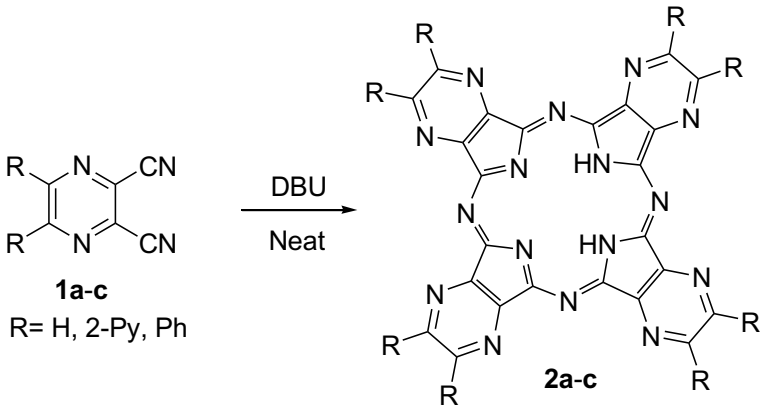

Ligands **2a-c** were obtained according to the procedure reported by Ercolani, Kadish *et al.* (Donzello, M. P.; Zhongping Ou, Z.; Monacelli, F.; Ricciardi, G.; Corrado Rizzoli, C.; Ercolani, C.; Kadish, K. M. *Inorg. Chem.* **2004**, *43*, 8626).

Pyrazinoporphyrazine macrocycles **2a-c** were prepared by autocyclotetramerization of starting materials **1a-c** as follows: the precursor (400 mg; 3.1 mmols) was placed in thick test tube and heated in a oil or sand bath until the solid melted (temperature of oil/sand bath employed: compound **1a**: 180°C; compound **1b**: 175°C; compound **1c**: 240°C). A few drops of DBU were added as catalyst. The mixture was manually stirred until a black solid was formed. After complete solidification, the solid was cooled down, finely grounded and purified by Soxhlet extraction with methanol (16 h) followed by acetone (10 h). The green or bluish powders were dried under vacuum until they reach a constant weight (Compound **2a**: blue powder, 21% yield; compound **2b**: green powder, 20% yield; compound **2c**: green powder, 18% yield).

2.5 *UV-Vis spectra of ligands **2a-c***

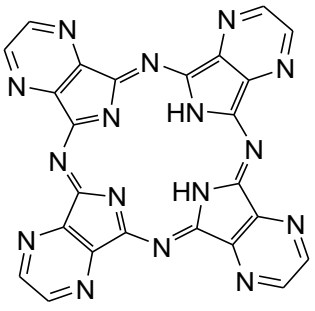

2a. UV-Vis in DMF: 636 nm, 576 nm, 435 nm, 404 nm.

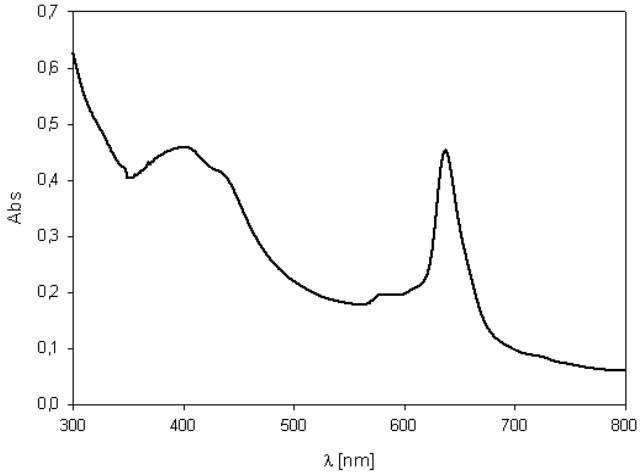

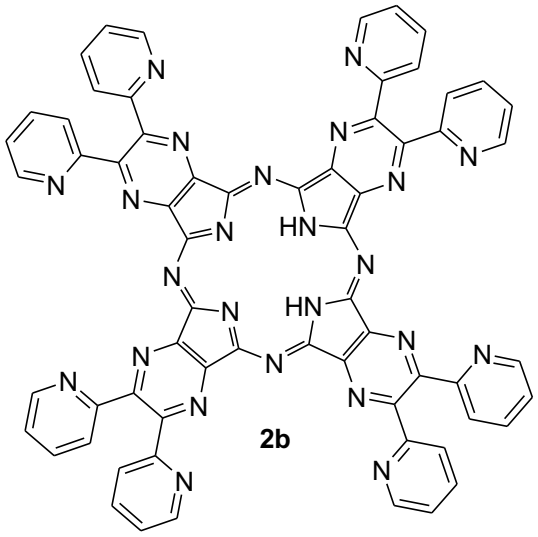

2b. UV-Vis in DCM: 668 nm, 634 nm, 617 nm, 605 nm, 581 nm, 421 nm, 355 nm.

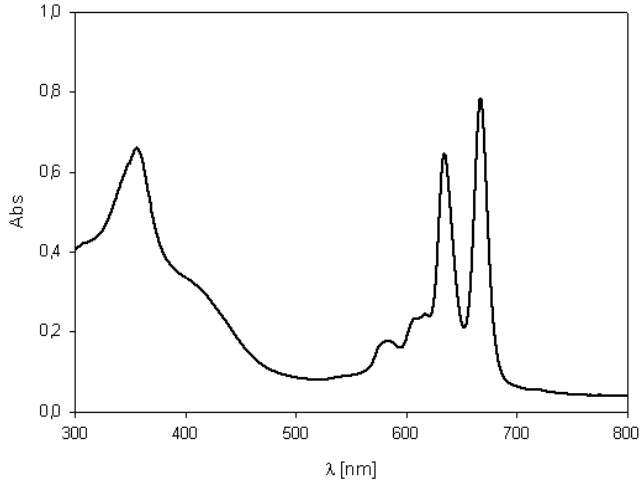

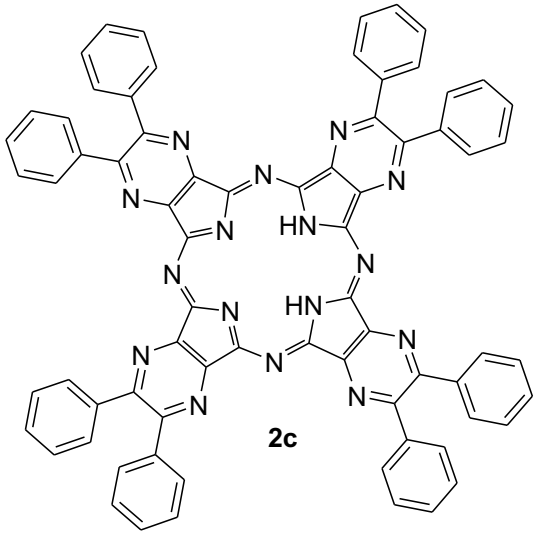

2c. UV-Vis in DMF: 657 nm, 336 nm.

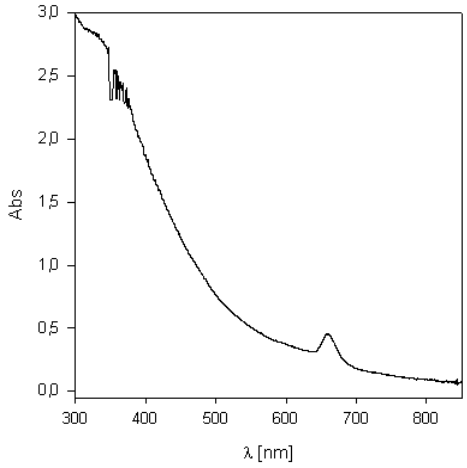

2c. UV-Vis in DCM: 667 nm, 638 nm, 342 nm.

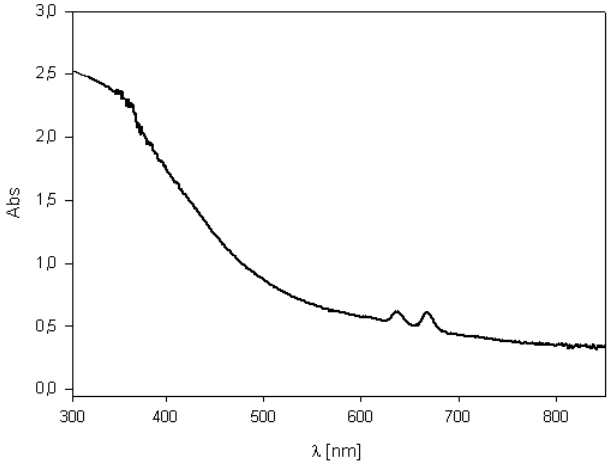

2.6 *General procedure for the preparation of Titanium-complexes **3a-c***

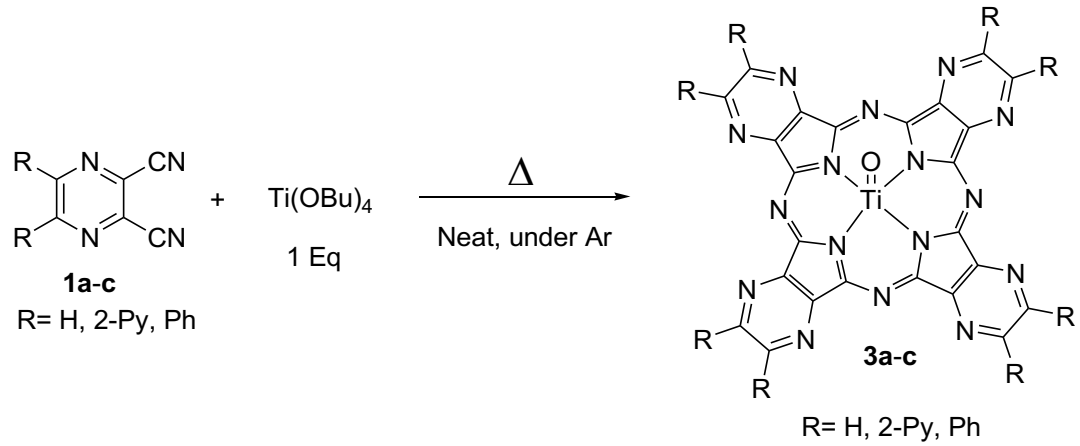

Titanium-based pyrazinoporphyrazines **3a-c** were prepared by cyclotetramerization of starting materials **1a-c** in the presence of titanium (IV) butoxide as follows: the precursor **1a-c** (400 mg; 3.1 mmols; 8 Equiv.) was placed under argon in a dry Schlenk flask and heated in a oil or sand bath until the solid melted (temperature of oil/sand bath employed: compound **1a**: 180°C; compound **1b**: 175°C; compound **1c**: 240°C). Against a flux of inert gas, titanium (IV) butoxide (0.39 mmols; 1 Equiv.) was added. The evolution of a white smoke was generally observed. The reaction mixture was stirred at high temperature (temperature of oil/sand bath employed: starting-material **1a**: 180°C; starting-material **1b**: 175°C; starting-material **1c**: 240°C) for 5 hours, then the mixture was cooled down, 30 mL of MeOH were added and the crude product was left under stirring overnight. The solid obtained was separated by centrifugation and brought to constant weight under vacuum. In order to dissolve the contaminants, the complex **3a-c** finely grounded, then resuspended in CH_2Cl_2 and left under stirring for 30 minutes. After this time, the product **3a-c** was collected by centrifugation and dried under vacuum until constant weight (Compound **3a**: blue powder; compound **3b**: green powder; compound **3c**: green powder). Products were obtained with the following yields: compound **3a** 78% yield; compound **3b** 65% yield; compound **3c** 95% yield.

*2.7 <u>UV-Vis spectra of Titanium-complexes **3a-c**</u>*

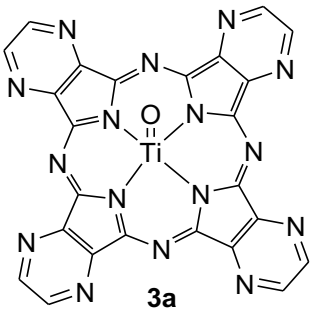

3a

3a. UV-Vis in DMF: 647 nm, 587 nm, 326 nm.

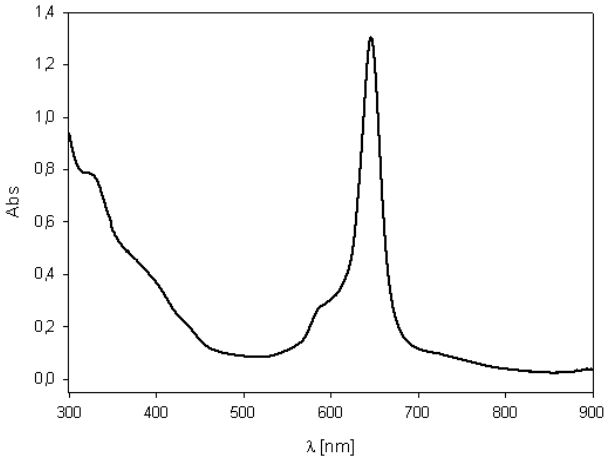

3a. UV-Vis in DCM: 646 nm, 614 nm, 585 nm, 338 nm.

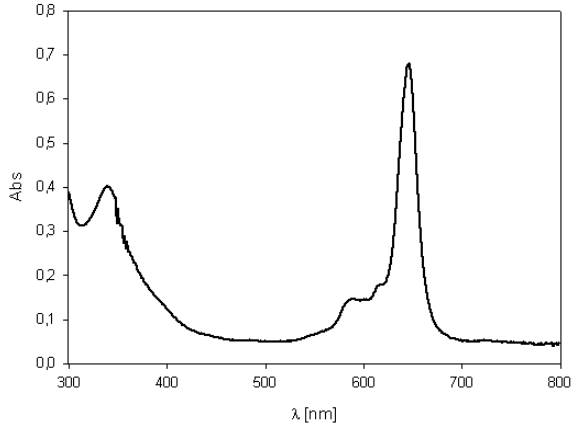

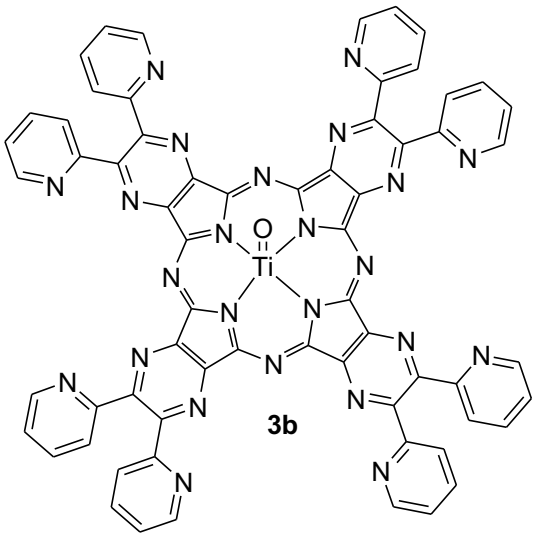

3b

3b. UV-Vis in DMF: 667 nm, 603 nm, 315 nm.

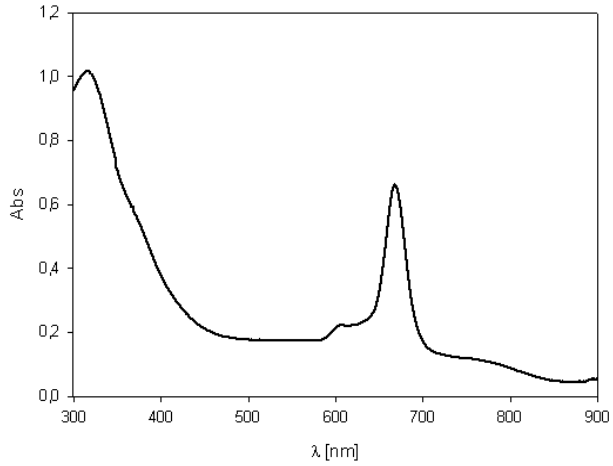

3b. UV-Vis in DCM: 668 nm, 634 nm, 605 nm, 577 nm, 320 nm.

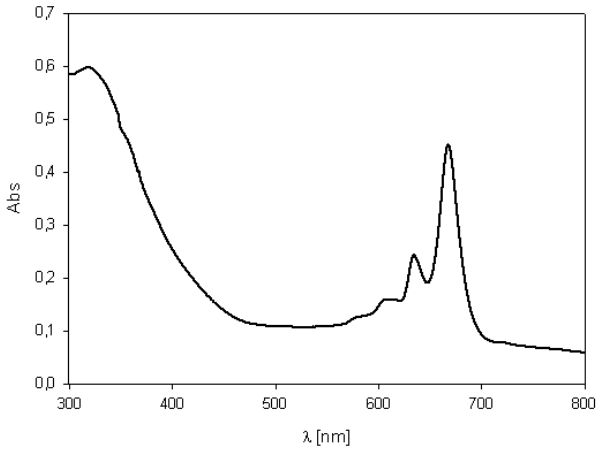

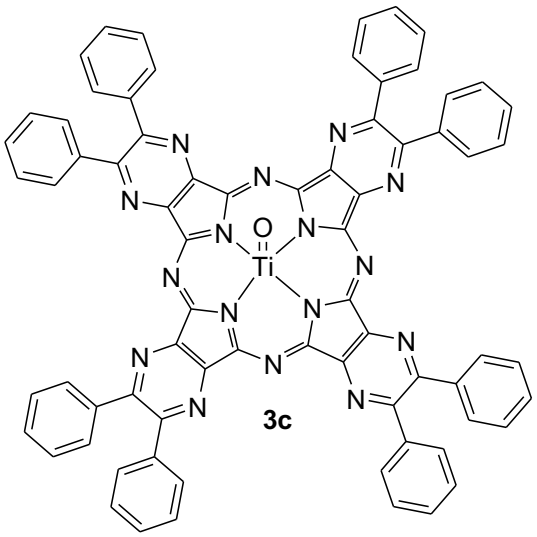

3c

3c. UV-Vis in DMF: 665 nm, 601 nm, 375 nm.

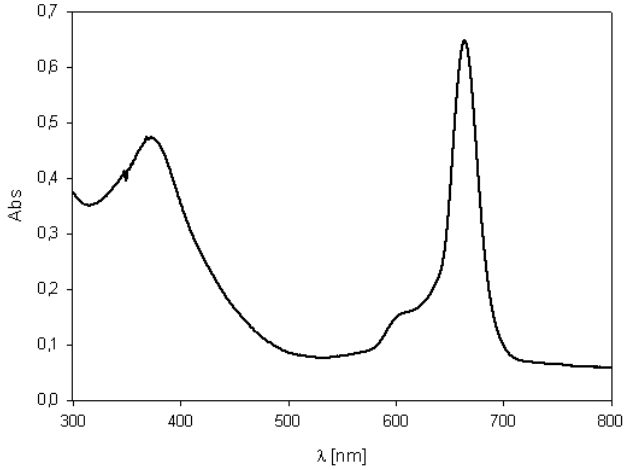

3c. UV-Vis in DCM: 666 nm, 637 nm, 607 nm, 445 nm, 362 nm.

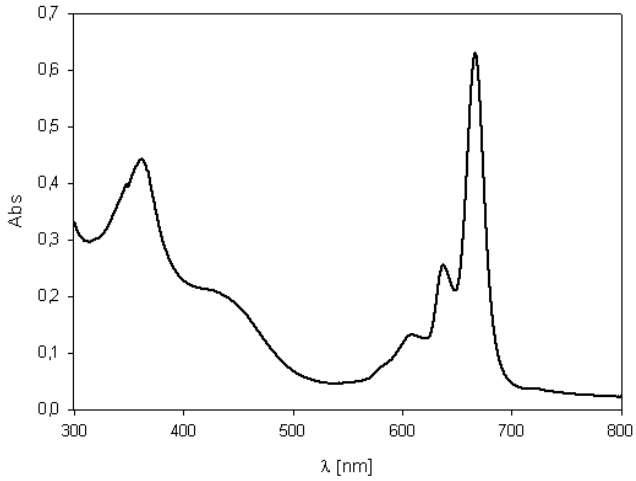

3. Cyclic voltammograms of ligands 2a-c and complexes 3a-c

Cyclic voltammetry was performed on a homemade electrochemical equipment consisting of a computer-controlled potentiostat with Vernier Software Multi Purpose Laboratory Interface (MPLI) program for Windows, a glassy-carbon disk (diameter of 1 mm) as working electrode; an Ag/AgCl/KCl 3 M as the reference electrode (E *vs* SCE = E *vs* Ag/AgCl -0.032), and a platinum disc (surface 1 cm^2) as the auxiliary electrode (Friis, E. P.; Andersen, J. E. T.; Madsen, L. L.; Bonander, N.; Moller, P.; Ulstrup, J. *Electrochim. Acta* **199**8, *43*, 1114). Cyclic voltammograms were acquired at 0.5 V/sec scan rate, 25°C, in DMF or DMSO containing Bu_4NBF_4 (0.1M) as supporting electrolyte. Concentration of ligands or complexes was 2 mM.

Titanium-based complexes **3a-c** were dissolved in 10 mL of DMSO/Bu_4NBF_4 0.1 M or DMF/Bu_4NBF_4 0.1 M, the solution was degassed with Argon then the voltammograms were recorded.

3.1 Cyclic voltammograms of ligands

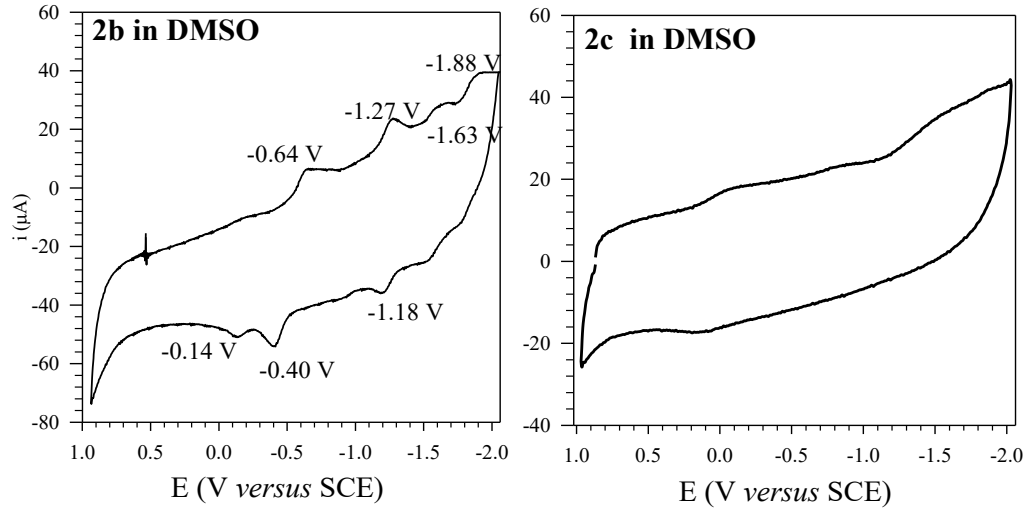

Cyclic voltammograms of ligand **2b** and **2c** in DMSO,0.1 M Bu_4NBF_4; scan rate 0.5 V/s

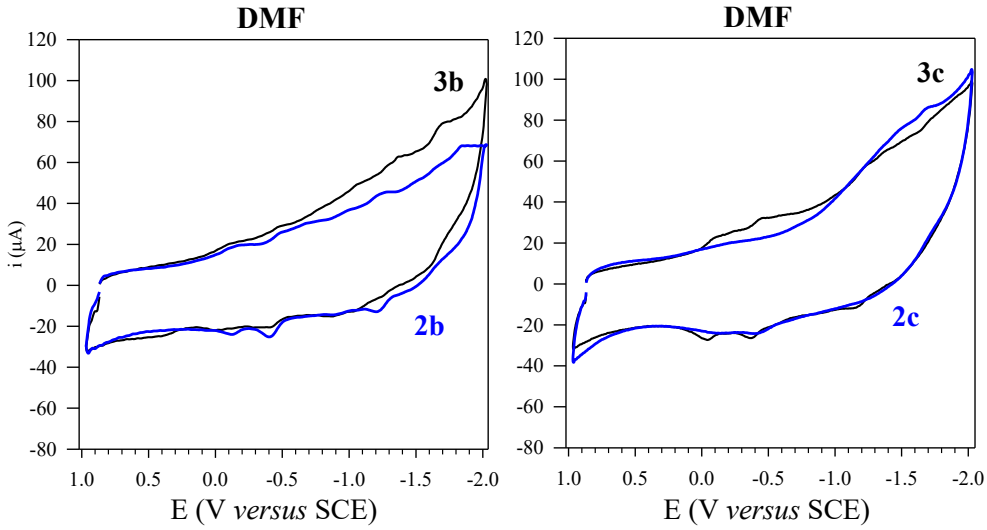

Cyclic voltammograms of complex **3b** and **3c** and their ligand**s 2b and 2c** in DMF, 0.1 M Bu_4NBF_4; scan rate 0.5 V/s

*3.2 Cyclic voltammograms of complex **3a** in DMSO*

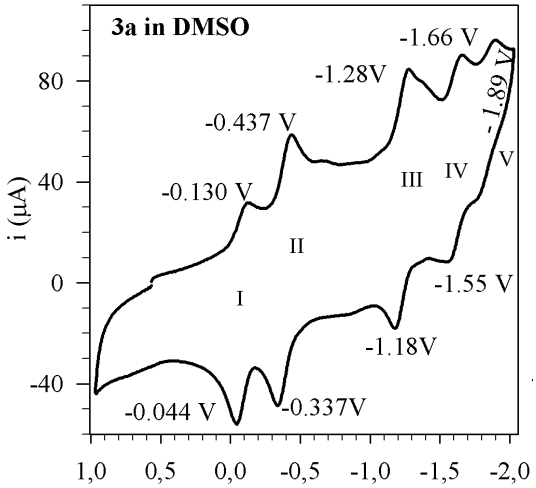

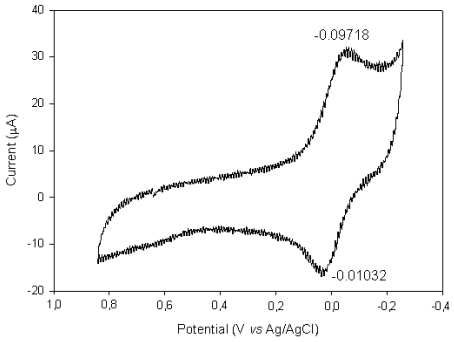

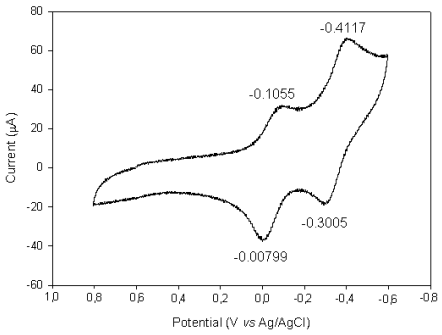

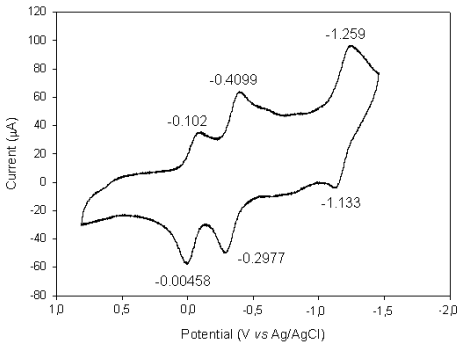

*3.3 Cyclic voltammograms of complex **3a** in DMF*

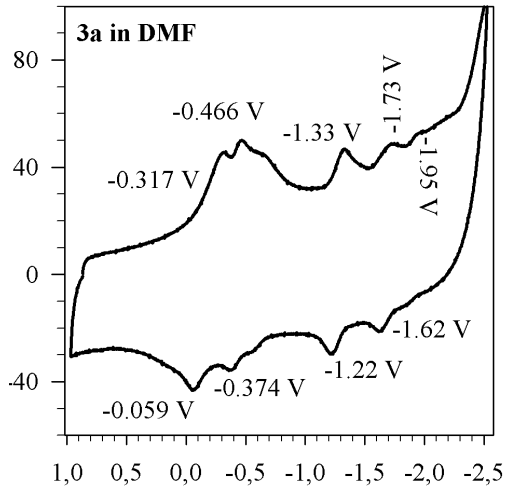

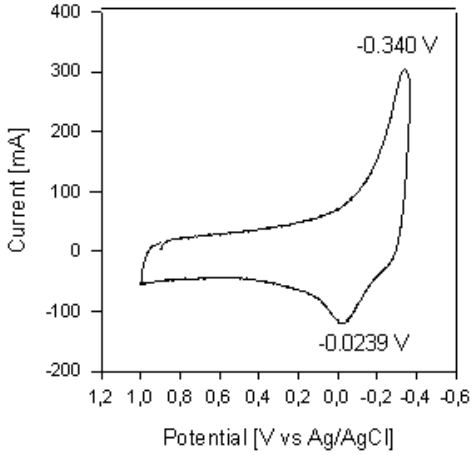

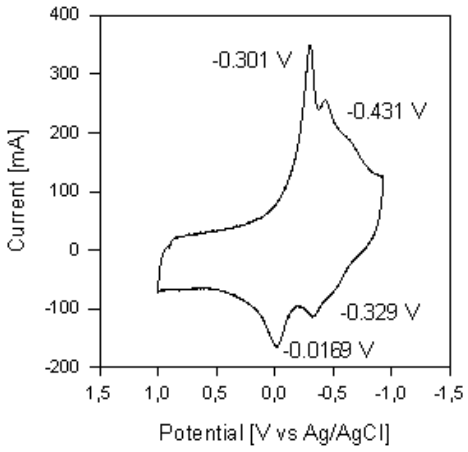

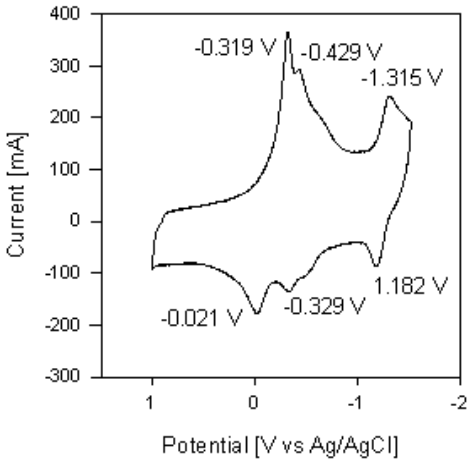

*3.4 Cyclic voltammograms of complex **3b** in DMSO*

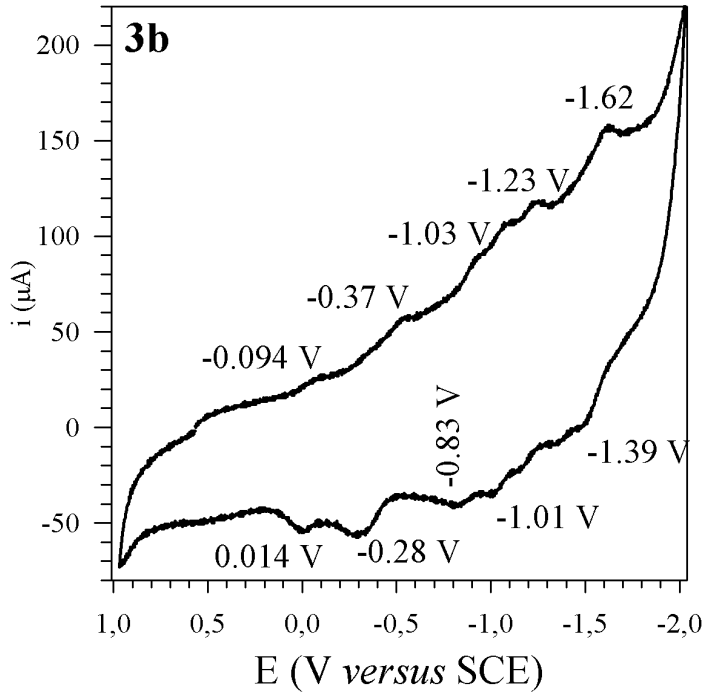

*3.5 Cyclic voltammograms of complex **3c** in DMSO*

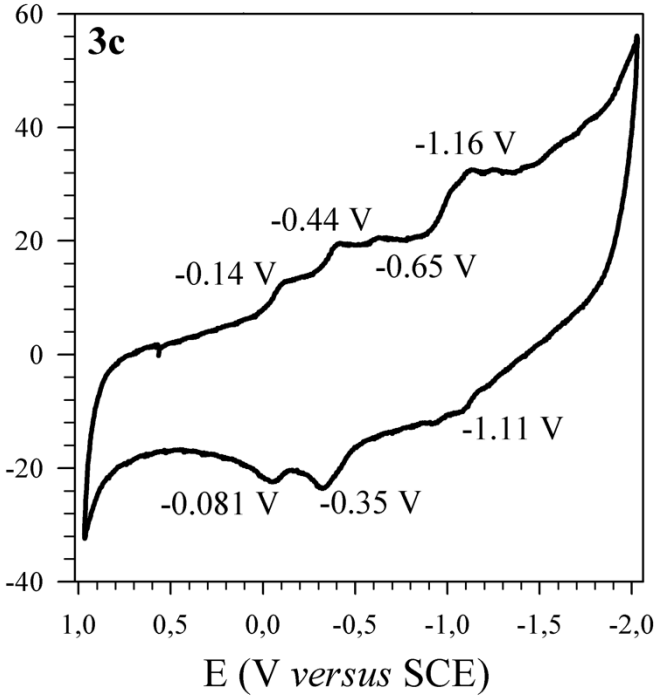

*3.6 Cyclic voltammograms of complex **3c** in DMF*

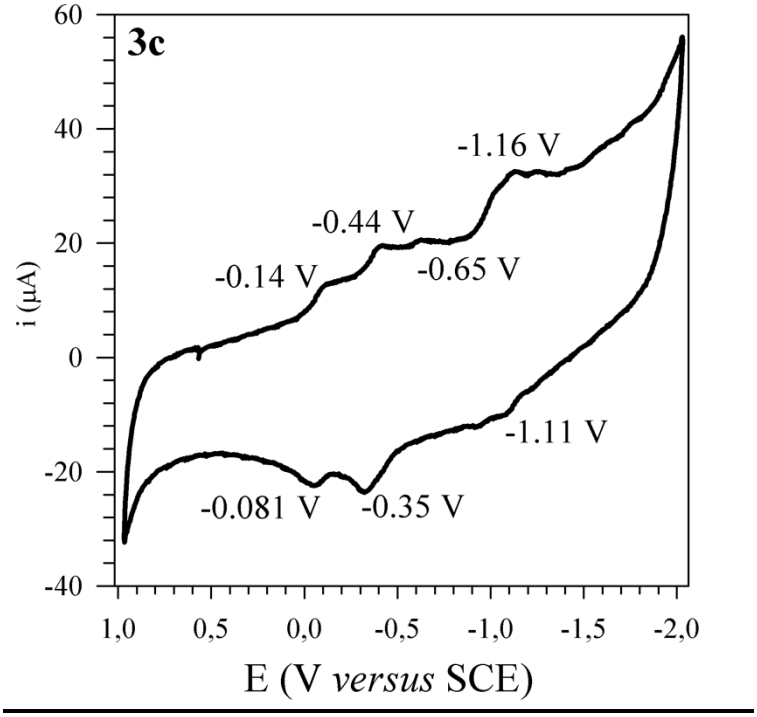

4. Solid State NMR: ^{1}H-^{13}C CP-MAS spectra of ligands 2a-c

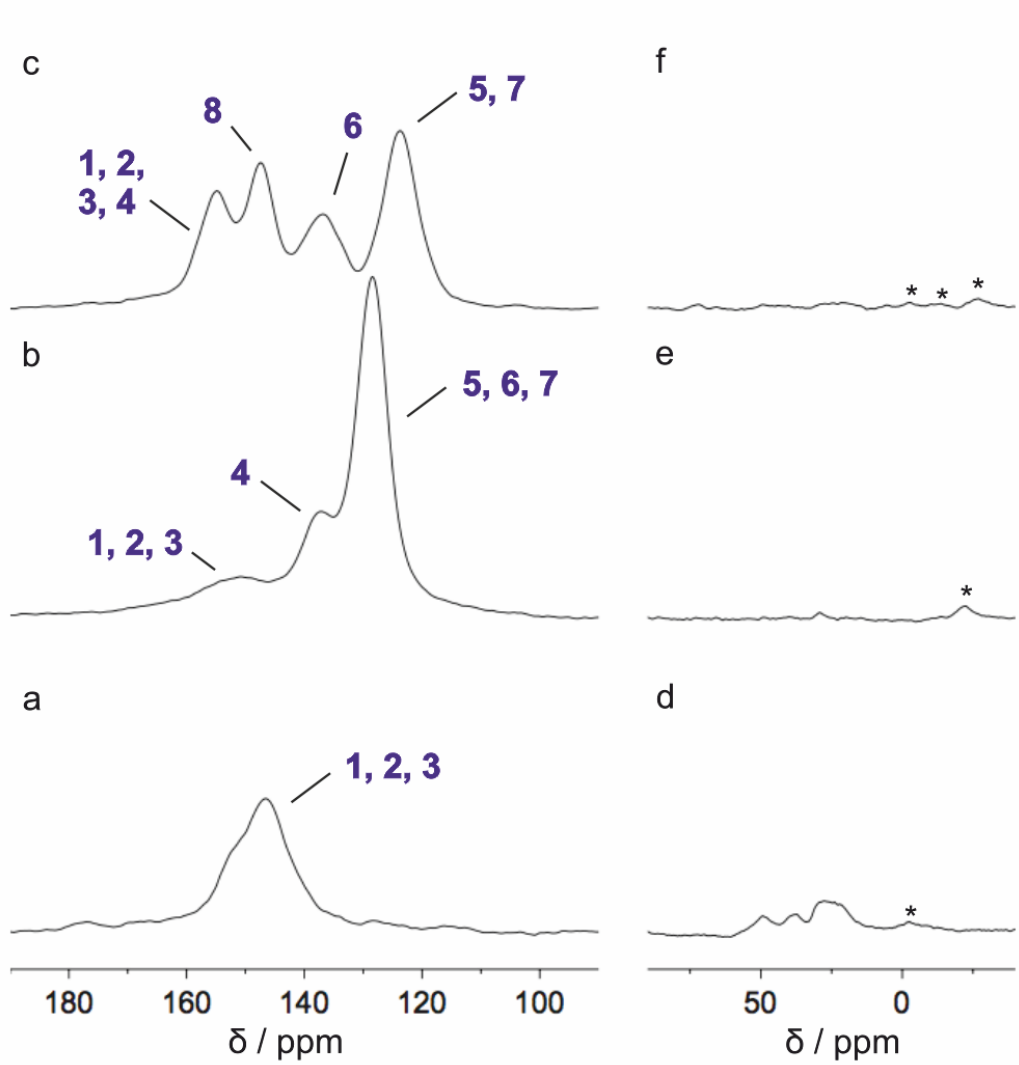

Aromatic (left panel) and aliphatic (right panel) regions of the ^{1}H-^{13}C CP-MAS spectra of ligands **2a** (a, d), **2c** (b, e) and **2b** (c, f). Spinning side bands are marked with asterisks.

5. MALDI-TOF analysis of ligands 2a-c and complexes 3a-c

In order to determine the mass of ligands and complexes a MALDI-TOF analysis was performed employing 2,5-dihydroxybenzoic acid (DHB) as matrix. The samples were prepared according to the following procedure (see references: Lidgard, R.; Duncan, M. W. *Rapid Commun. Mass Sp.* **1995**, *9*, 128; Canlica, M.; nyokong, T. *Polyedron* **2011**, *30*, 1975):

- A standard solution of DHB matrix was prepared dissolving 0.14 mmols of DBH in 1 mL of CH_3CN 100% (standard solution A);
- A standard solution for each ligand and complex was prepared dissolving $2*10^{-3}$ mmols of ligand/complex in 1 mL of CH_3CN 100% (standard solution B);
- Standard solution A was diluted 1:100 with CH_3CN 100% (standard solution C);
- Standard solution B was diluted 1:10 with CH_3CN 100% (standard solution D);
- 6 µL of standard solution C were mixed with 9 µL of standard solution D (solution E);
- 0.5 µL of solution E were applied on the MALDI plate. The solvent was let to evaporate in order to form a crystal.
- The MALDI plate was transferred inside the instrument for the analysis.
- The spectra were acquired in the positive reflector mode by 20 subspectral accumulations (each consisting of 50 laser shots) in an 50-1000 mass range, focus mass 600 Da, using a 351 nm Nb:YAG laser with a 20 kV acceleration voltage.

5.1 Mass spectrum of the DHB matrix (full spectrum)

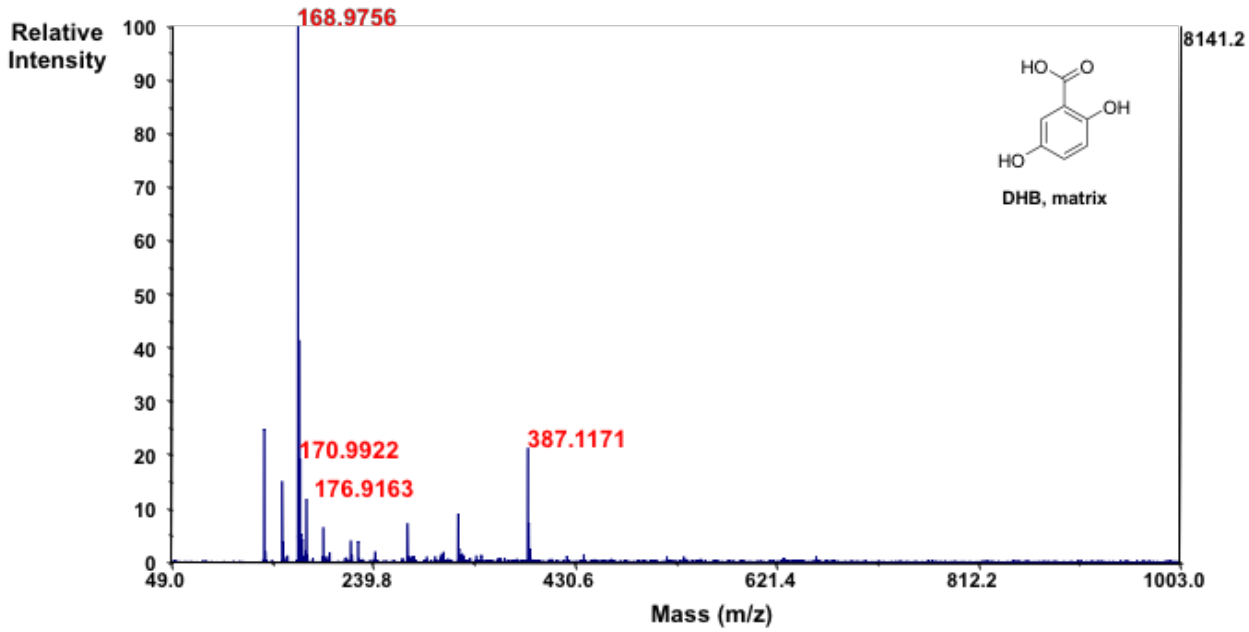

*5.2 Mass spectrum of ligand **2a***

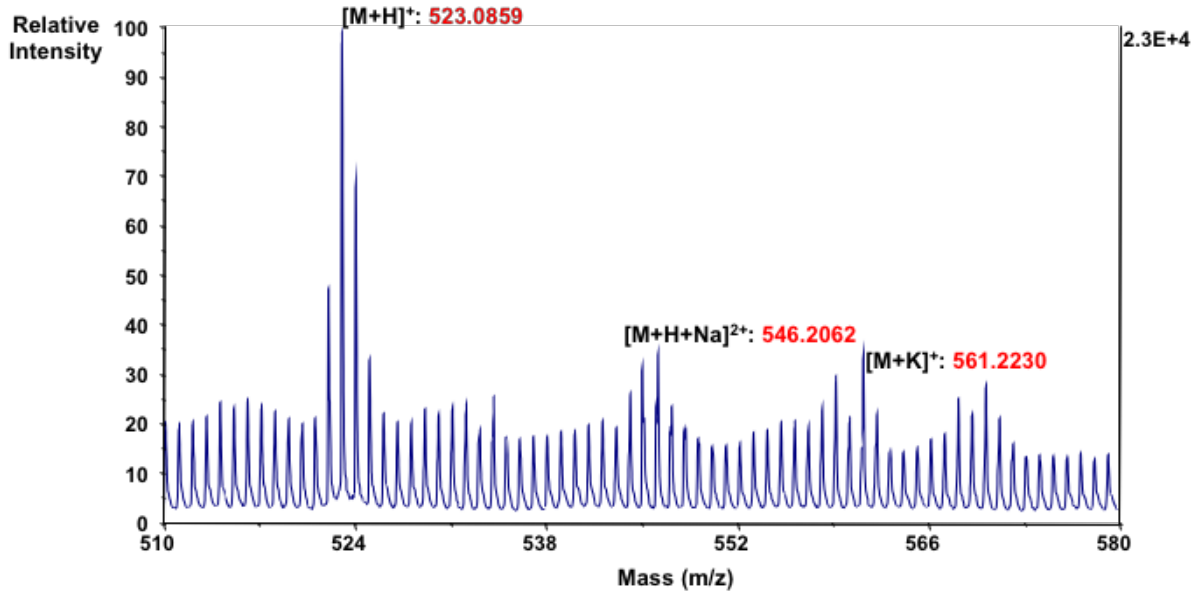

---

*5.3 Mass spectrum of ligand **2a**: enlargement and comparison with the matrix DHB*

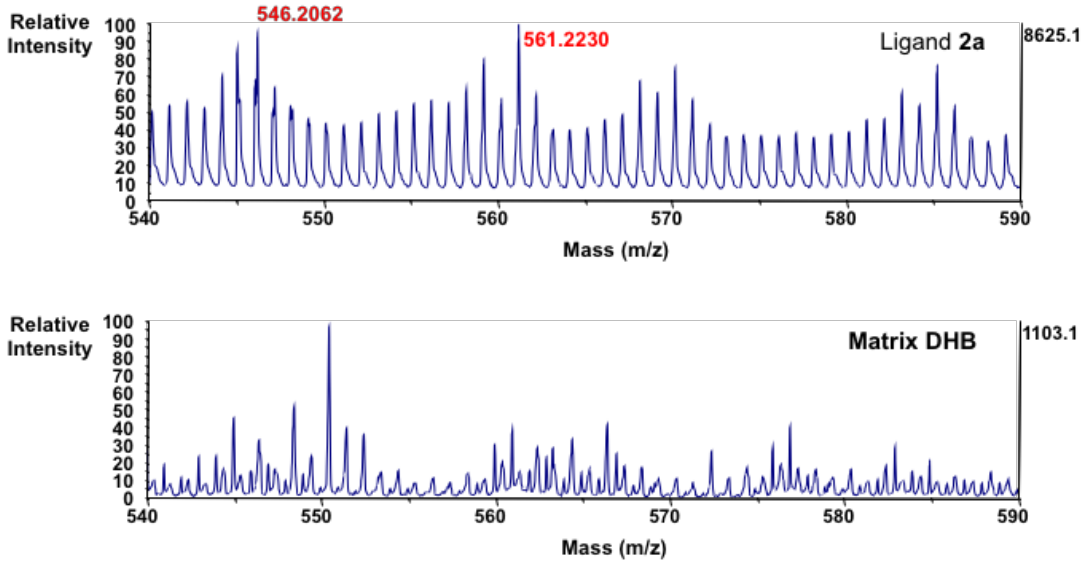

---

*5.4 Mass spectrum of ligand **2b***

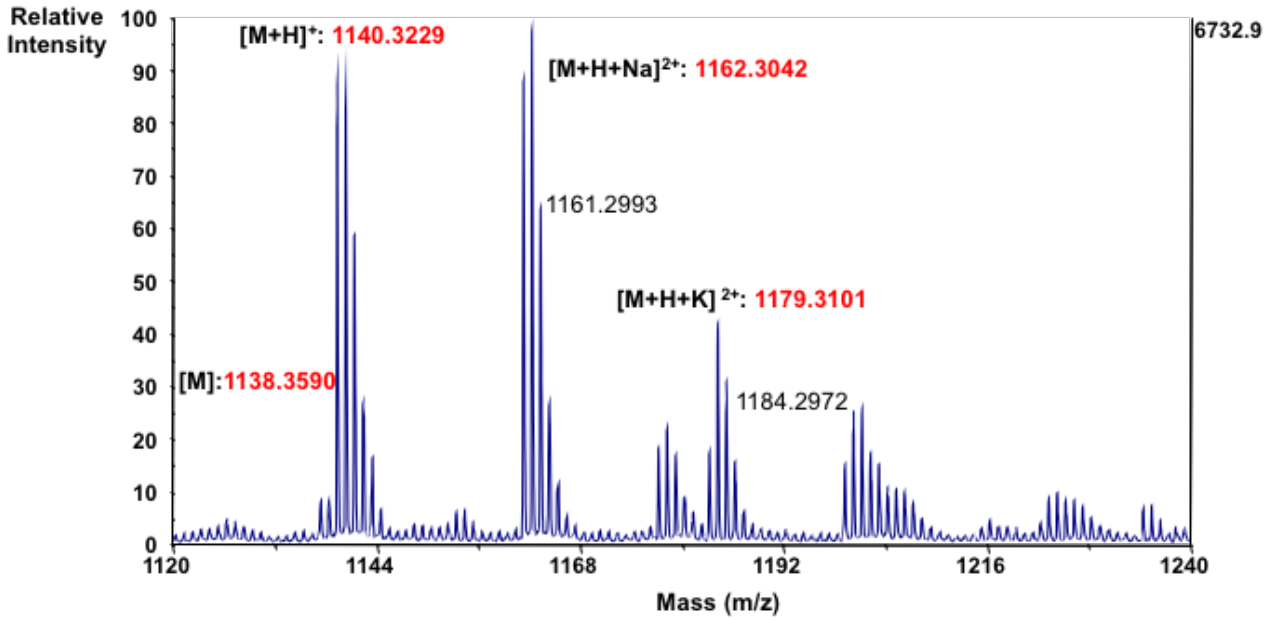

*5.5 Mass spectrum of ligand **2b**: enlargement and comparison with the matrix DHB*

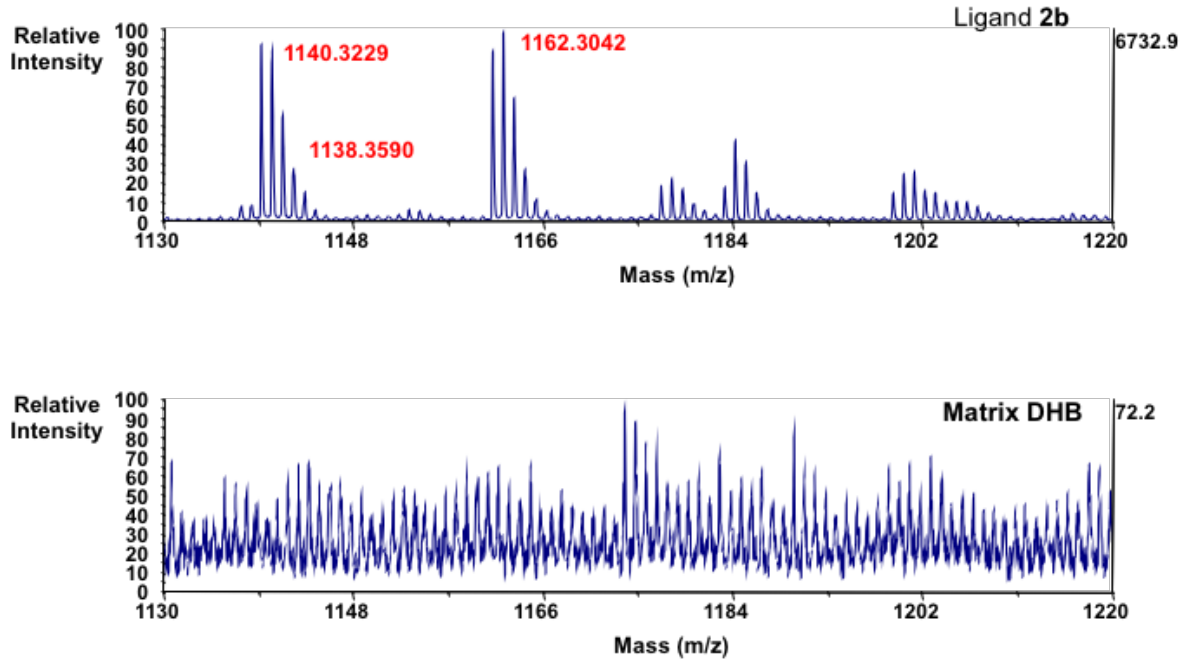

*5.6 Mass spectrum of ligand **2c***

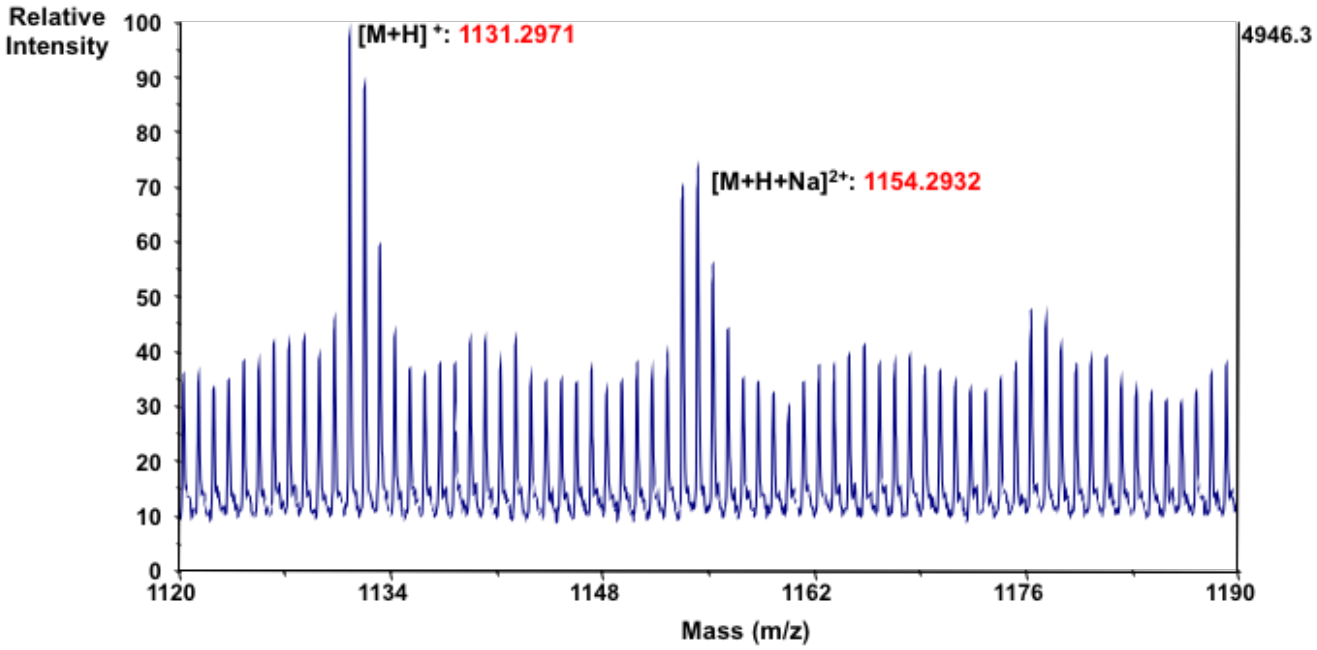

*5.7 Mass spectrum of ligand **2c**: enlargement and comparison with the matrix DHB*

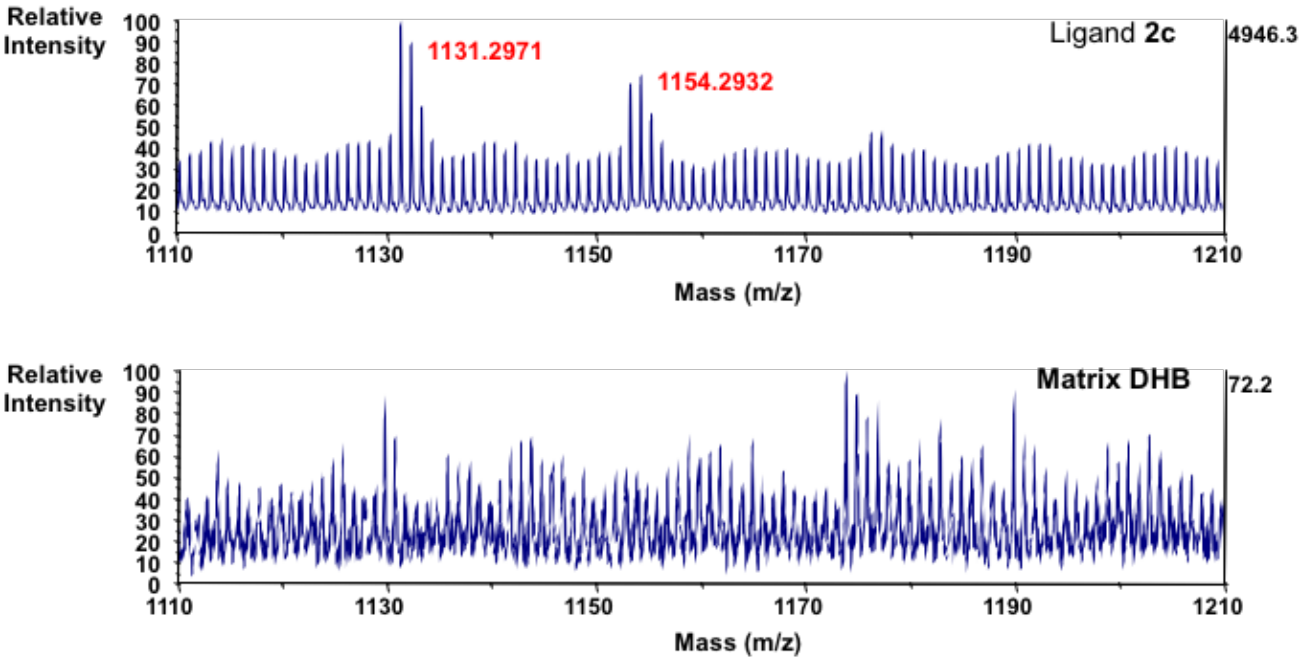

*5.8 Mass spectrum of complex **3a***

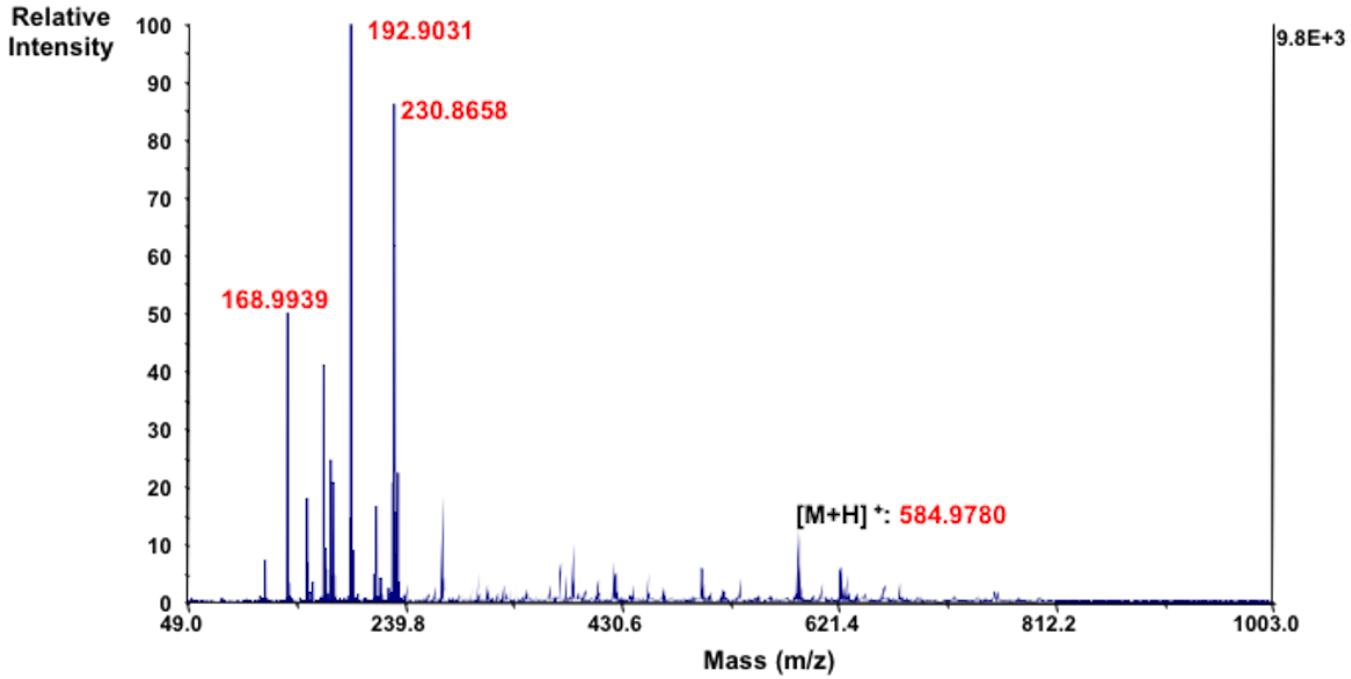

*5.9 Mass spectrum of ligand **3a**: enlargement and comparison with the matrix DHB*

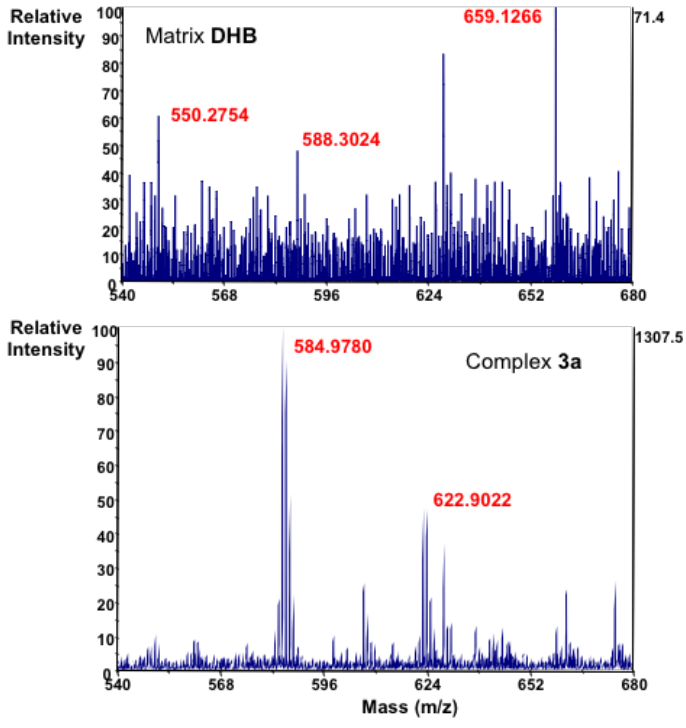

5.10 *Mass spectrum of complex **3b***

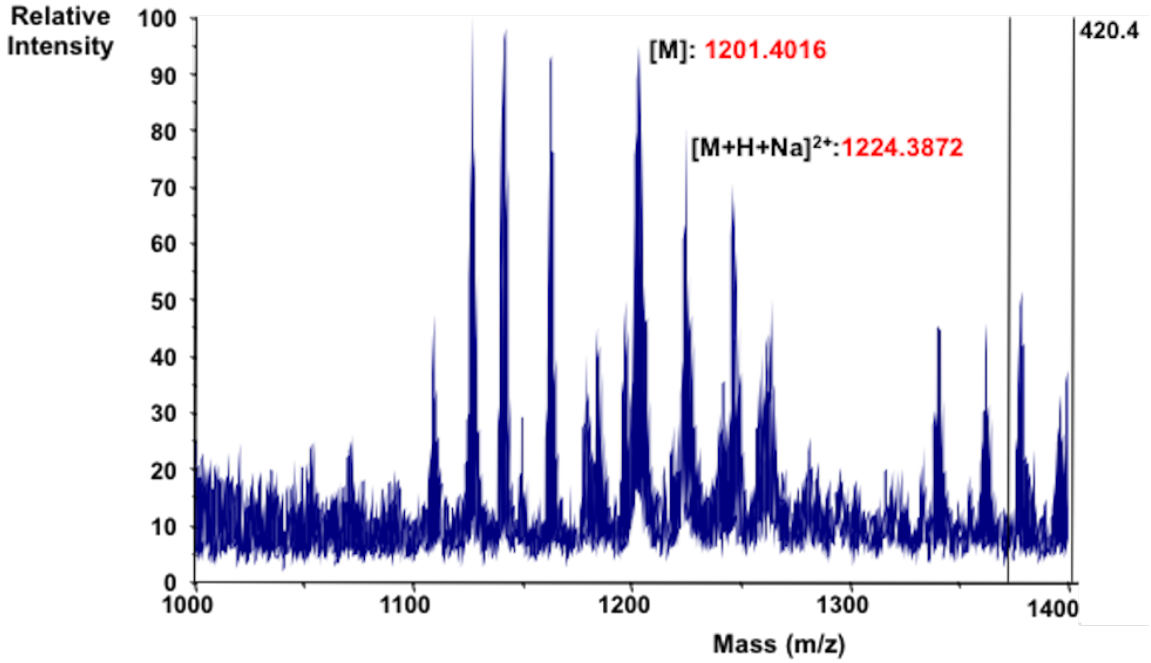

5.11 *Mass spectrum of ligand **3b**: enlargement and comparison with the matrix DHB*

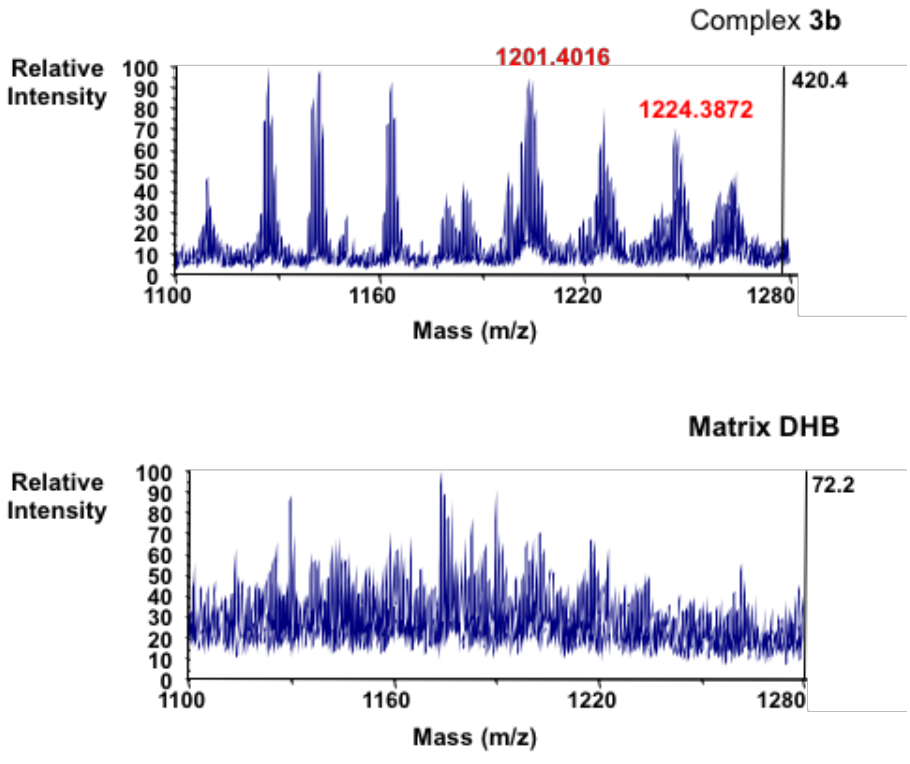

*5.12 Mass spectrum of the complex **3c***

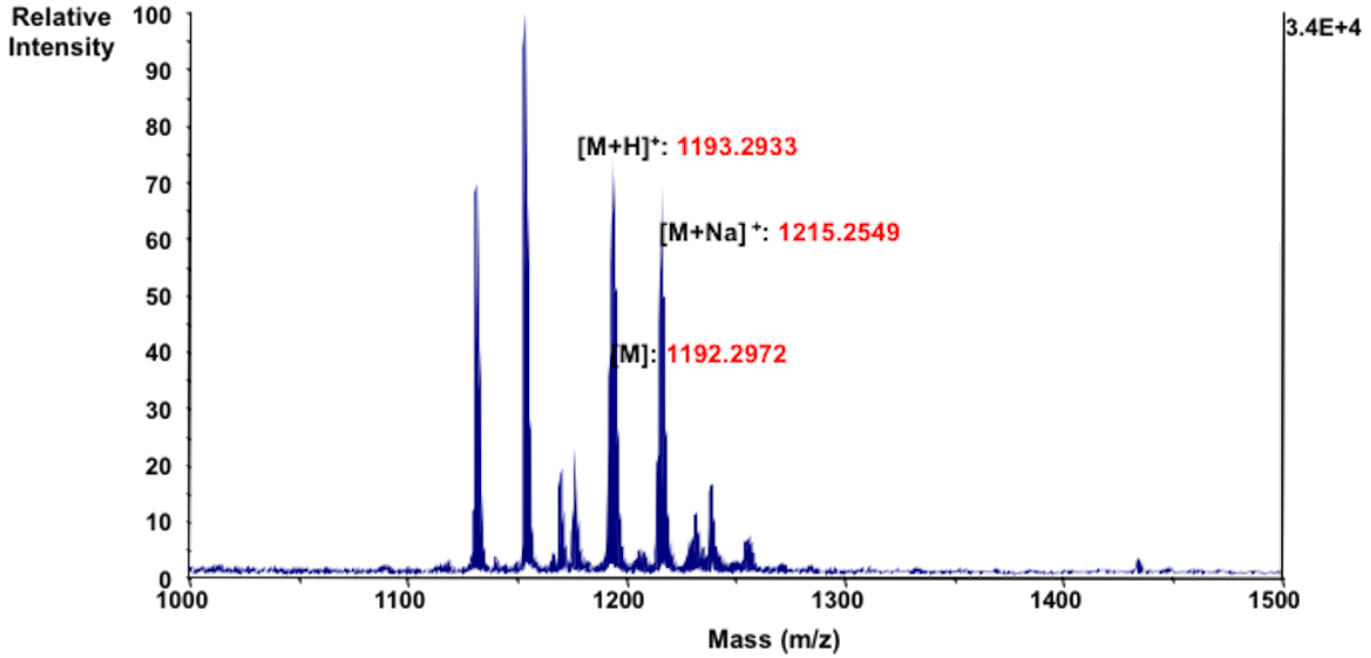

*5.13 Mass spectrum of ligand **3c**: enlargement and comparison with the matrix DHB*

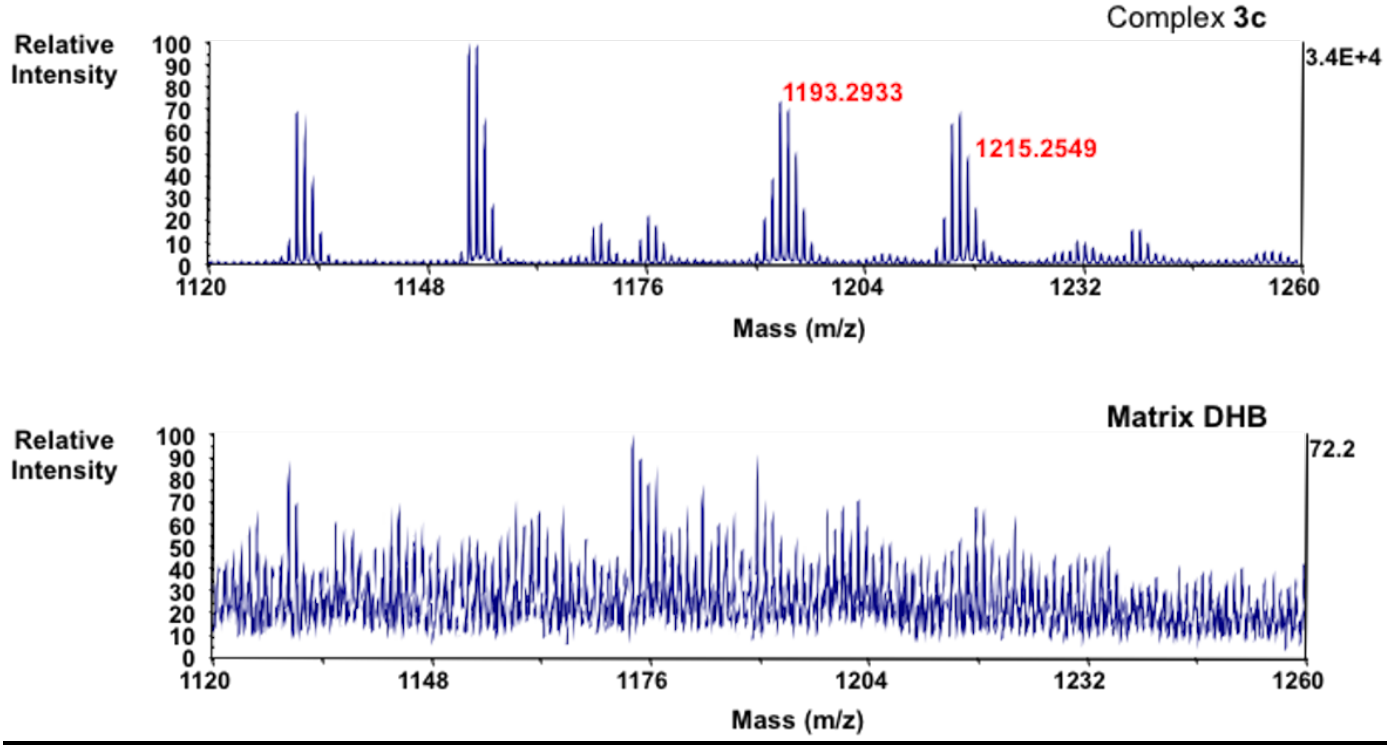

Sample name	MALDI-TOF adduct	Mass found	Mass calculated
Ligand **2a**	$[M+H]^+$ $[M+H+Na]^{2+}$ $[M+H+K]^{2+}$	523.0859 546.2062 561.2230	523.1353 546.1250 561.0990
Ligand **2b**	[M] $[M+H]^+$ $[M+H+Na]^{2+}$ $[M+H+K]^{2+}$	1138.3590 1140.3229 1162.3042 1179.3101	1138.3398 1139.3477 1162.3374 1179.2218
Ligand **2c**	$[M+H]^+$ $[M+H+Na]^{2+}$	1131.2971 1154.2932	1131.3857 1154.3754
Complex **3a**	$[M+H]^+$	584.9780	585.0625
Complex **3b**	[M] $[M+H+Na]^{2+}$	1201.4016 1224.3872	1200.2670 1224.2646
Complex **3c**	[M] $[M+H]^+$ $[M+Na]^+$	1192.2972 1193.2933 1215.2549	1192.3050 1193.3129 1216.3026

6. IR spectra of ligands 2a-c and complexes 3a-c

*6.1 IR spectra of ligands **2a***

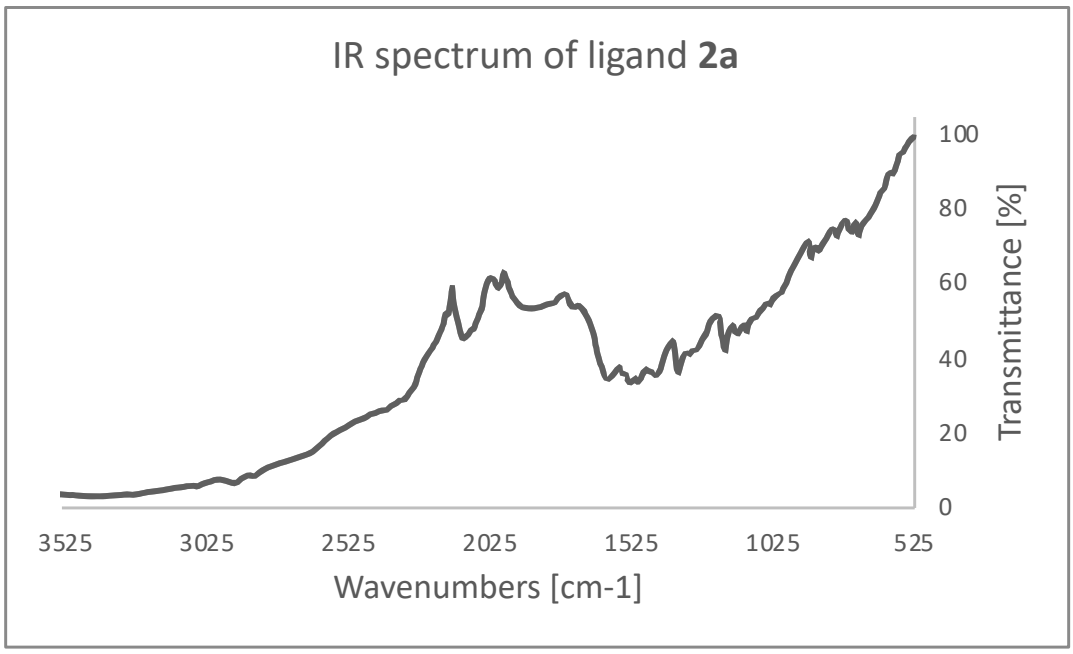

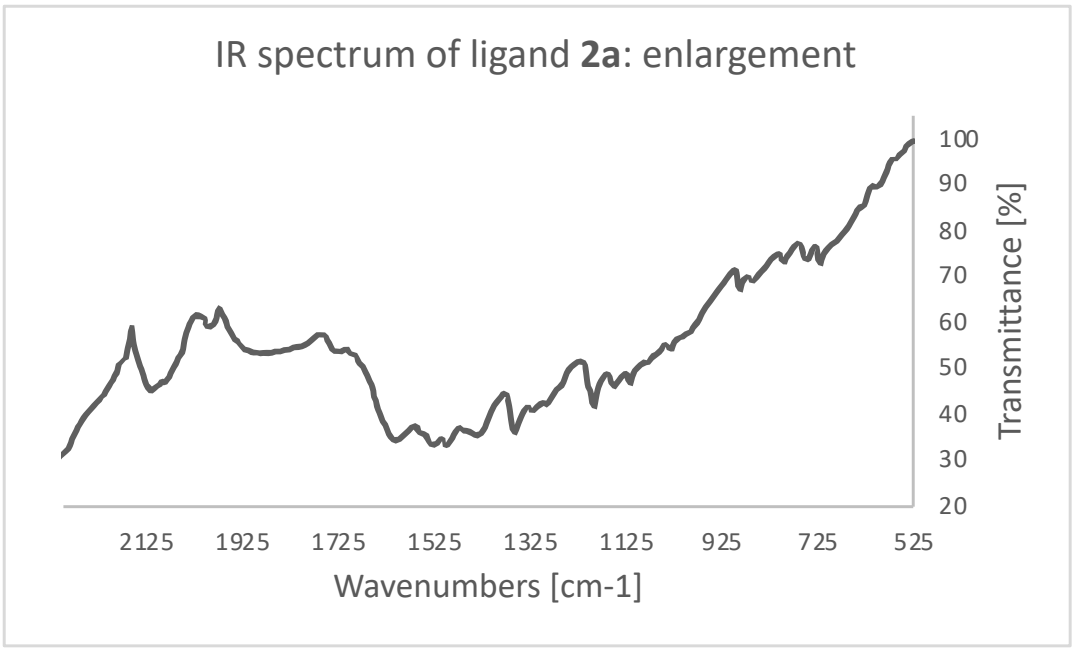

IR spectrum of ligand **2a**: 722 cm^{-1}; 725 cm^{-1}; 857 cm^{-1}; 890 cm^{-1}; 1150 cm^{-1}; 1118 cm^{-1}; 1193 cm^{-1}; 1356 cm^{-1}; 1429 cm^{-1}; 1599 cm^{-1}; 1868 cm^{-1}; 2111 cm^{-1}; 2936 cm^{-1}.

6.2 *IR spectra of ligands* ***2b***

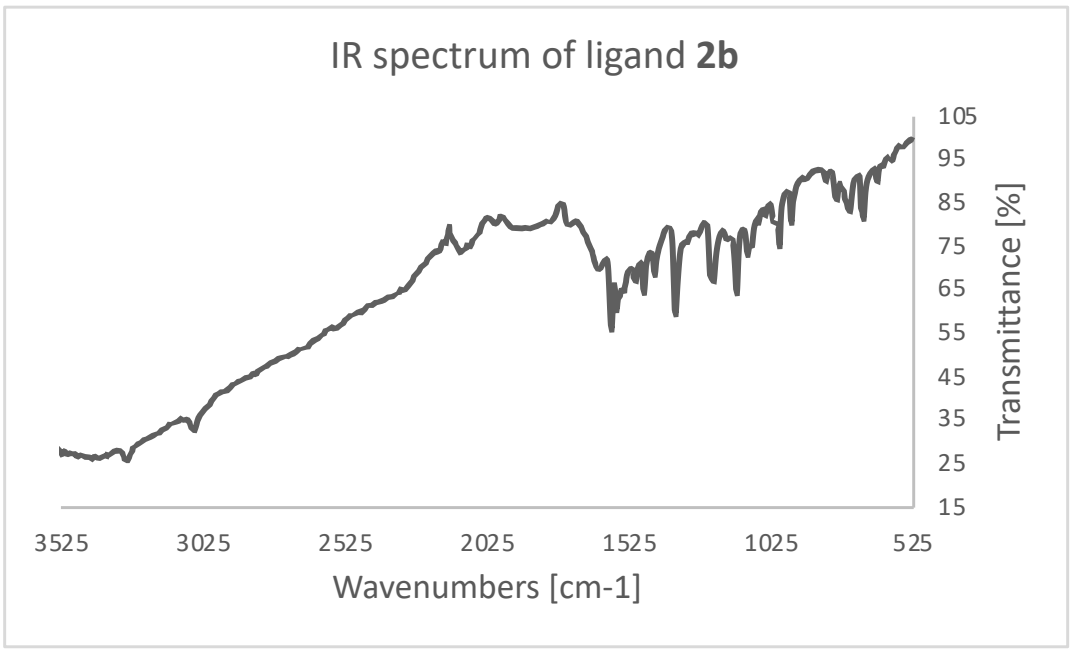

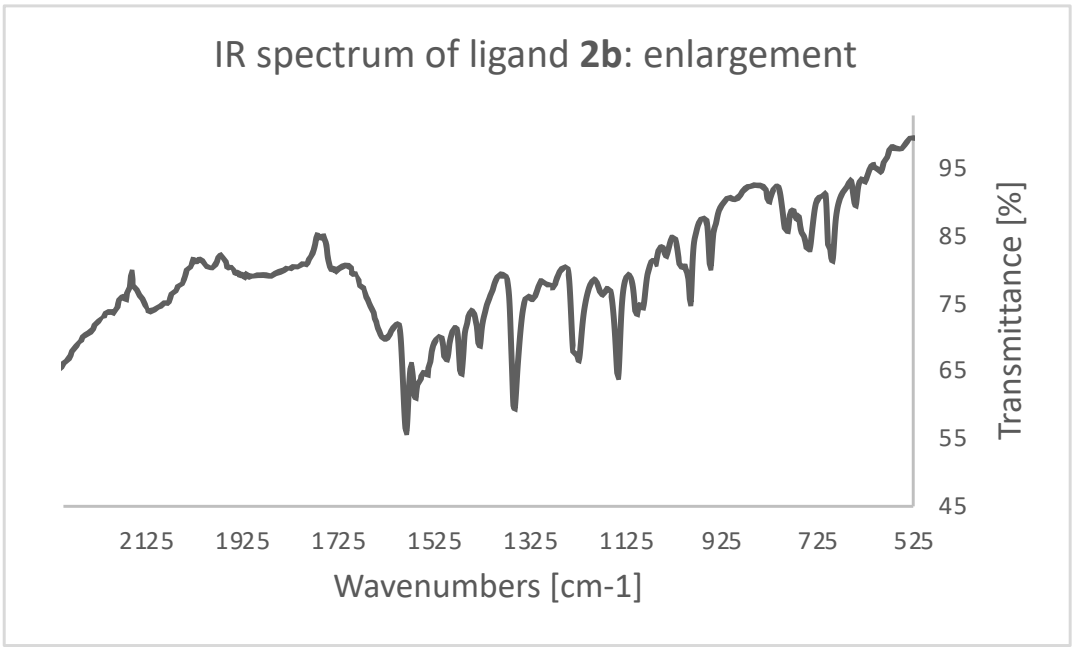

IR spectrum of ligand **2b**: 648 cm^{-1}; 696 cm^{-1}; 744 cm^{-1}; 759 cm^{-1}; 801 cm^{-1}; 950 cm^{-1}; 992 cm^{-1}; 1092 cm^{-1}; 1105 cm^{-1}; 1144 cm^{-1}; 1225 cm^{-1}; 1360 cm^{-1}; 1431 cm^{-1}; 1470 cm^{-1}; 1500 cm^{-1}; 1585 cm^{-1}; 1566 cm^{-1}; 1864 cm^{-1}; 2096 cm^{-1}; 3052 cm^{-1}; 3285 cm^{-1}.

6.3 *IR spectra of ligands **2c***

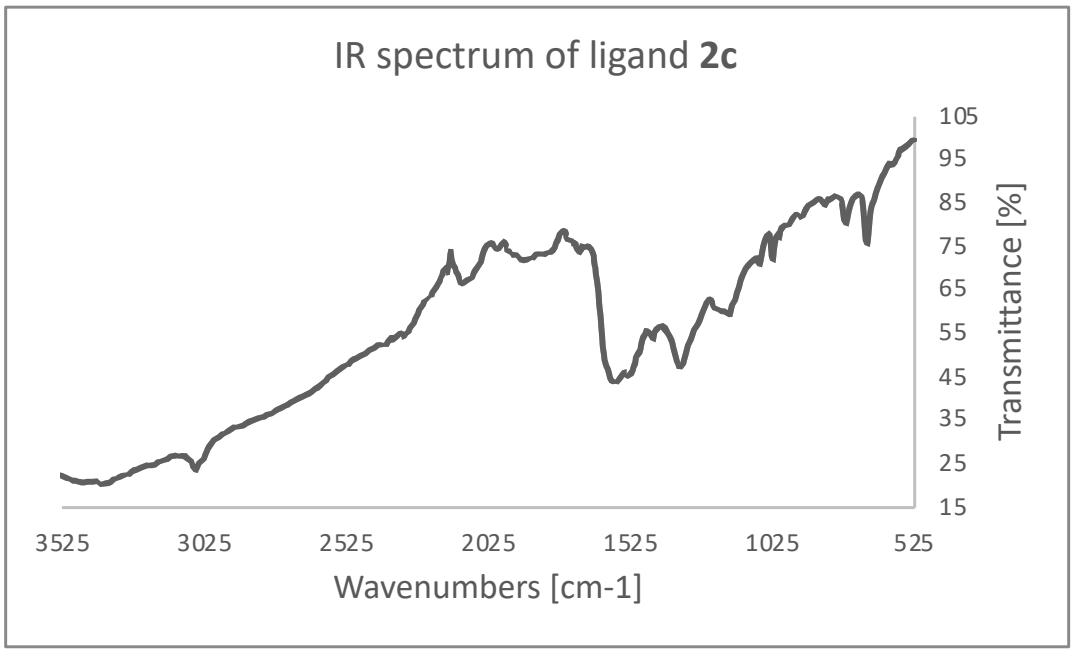

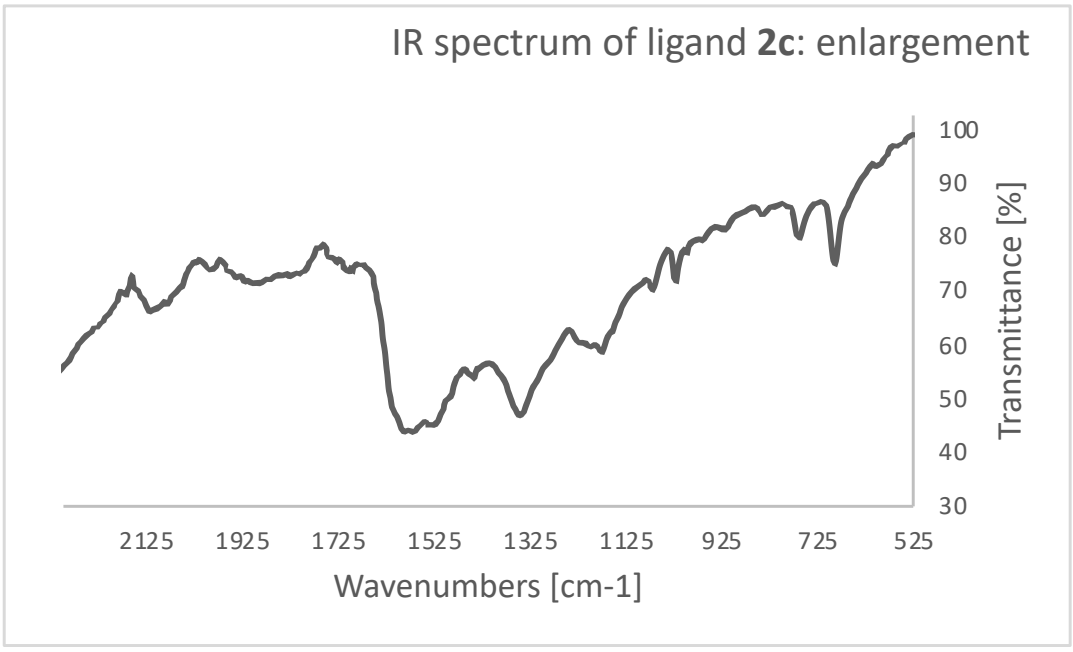

IR spectrum of ligand **2c**: 689 cm^{-1}; 765 cm^{-1}; 1023 cm^{-1}; 1173 cm^{-1}; 1340 cm^{-1}; 1523 cm^{-1}; 1860 cm^{-1}; 2103 cm^{-1}; 3053 cm^{-1}.

6.4 *IR spectra of complex **3a***

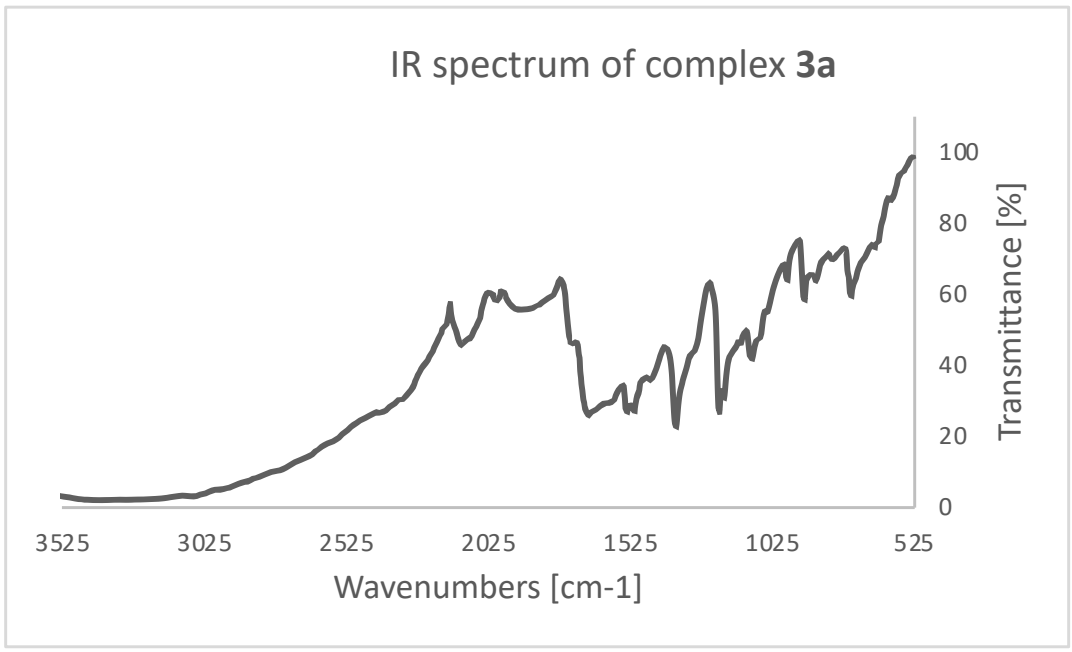

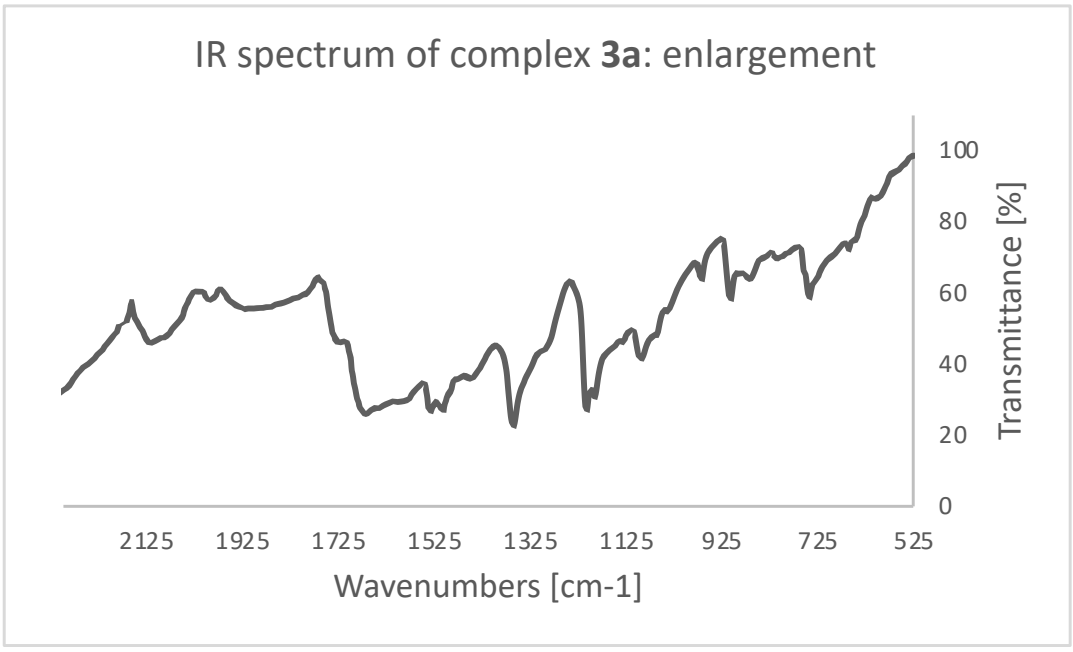

IR spectrum of ligand **3a**: 744 cm^{-1}; 906 cm^{-1}; 909 cm^{-1}; 913 cm^{-1}; 1208 cm^{-1}; 1359 cm^{-1}; 1507 cm^{-1}; 1508 cm^{-1}; 1664 cm^{-1}; 1864 cm^{-1}; 2110 cm^{-1}.

6.5 *IR spectra of complex **3b***

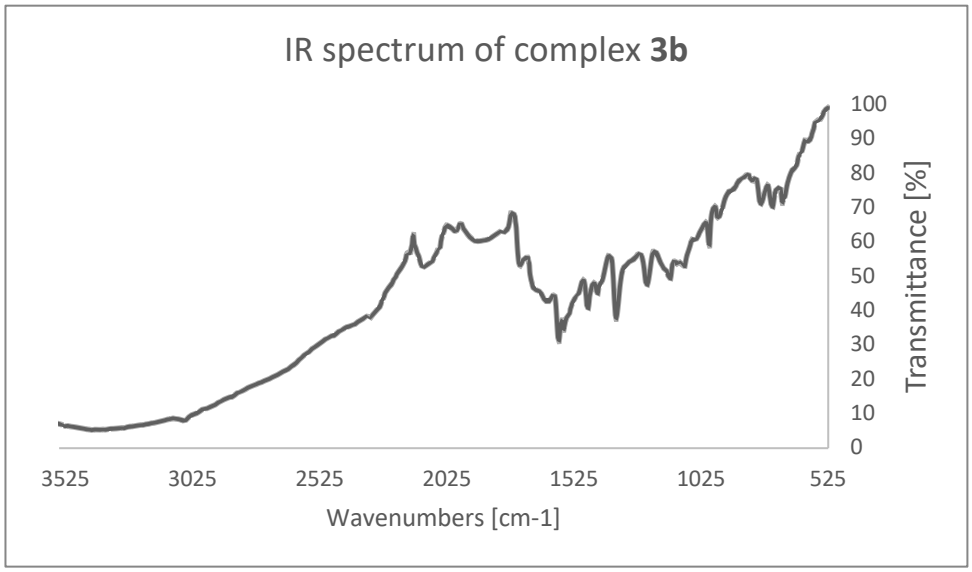

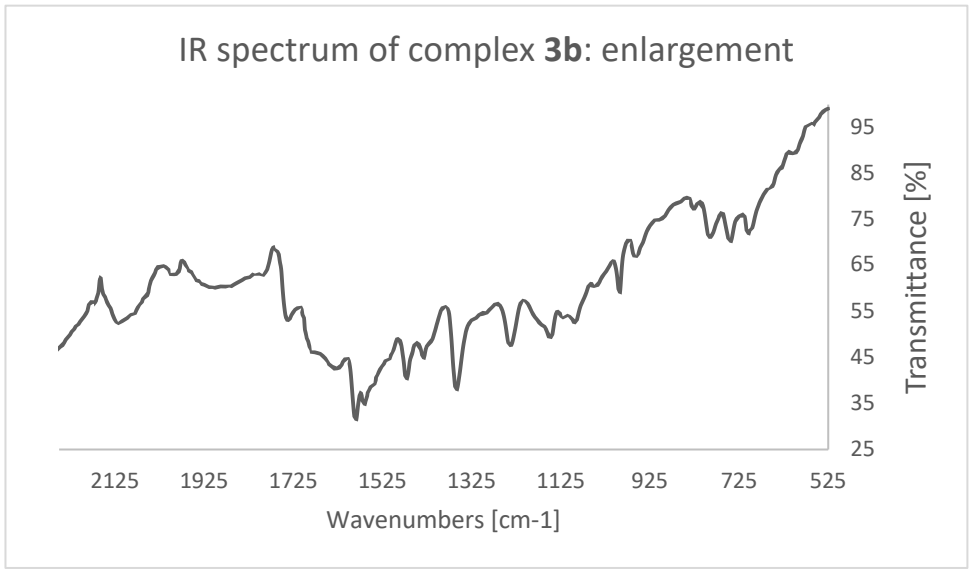

IR spectrum of complex 3**b**: 705 cm^{-1}; 744 cm^{-1}; 790 cm^{-1}; 958 cm^{-1}; 993 cm^{-1}; 1092 cm^{-1}; 1147 cm^{-1}; 1359 cm^{-1}; 1432 cm^{-1}; 1471 cm^{-1}; 1566 cm^{-1}; 1584 cm^{-1}; 1738 cm^{-1}; 2113 cm^{-1}.

6.6 *IR spectra of complex **3c***

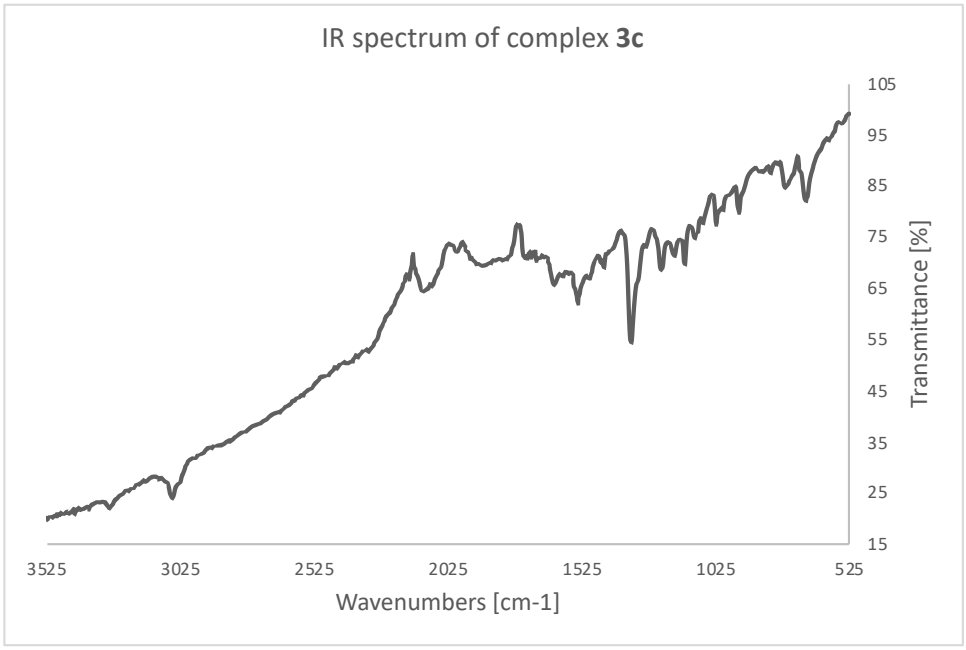

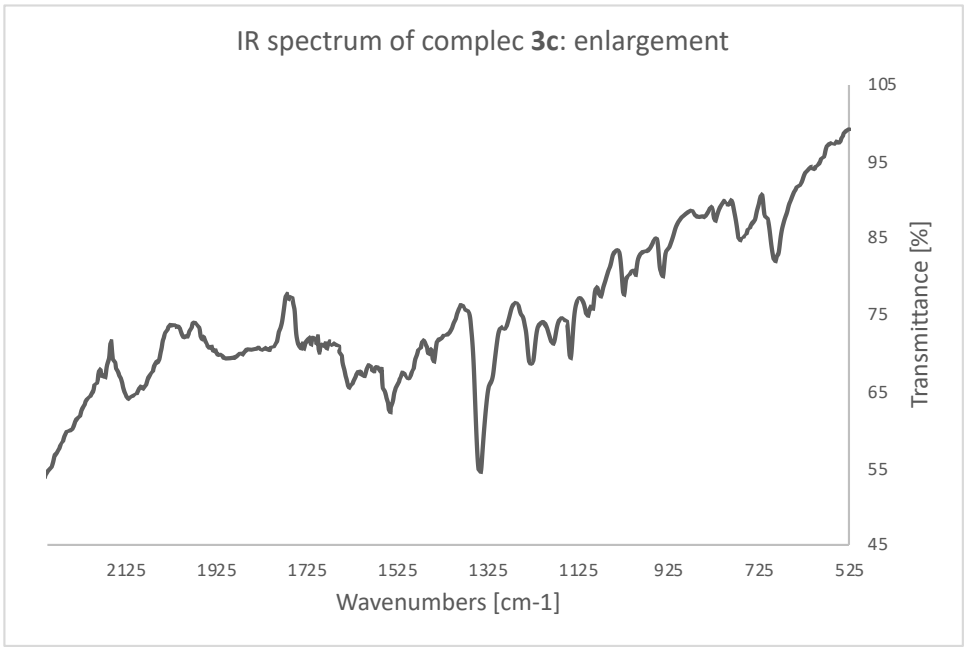

IR spectrum of complex **3c**: 690 cm^{-1}; 768 cm^{-1}; 938 cm^{-1}; 1024 cm^{-1}; 1104 cm^{-1}; 1143 cm^{-1}; 1180 cm^{-1}; 1231 cm^{-1}; 1341 cm^{-1}; 1444 cm^{-1}; 1540 cm^{-1};1631 cm^{-1}; 1885 cm^{-1}; 2102 cm^{-1}; 3051 cm^{-1}; 3288 cm^{-1}.

7. SEM images of complexes 3a-c

*7.1 SEM images of complex **3a***

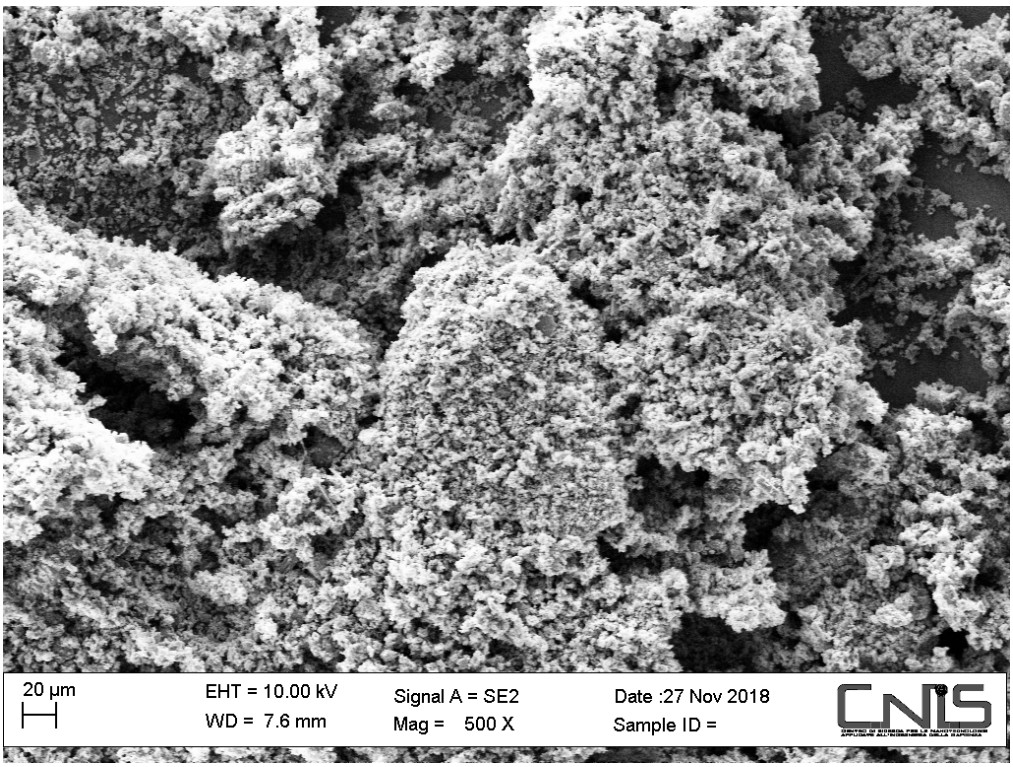

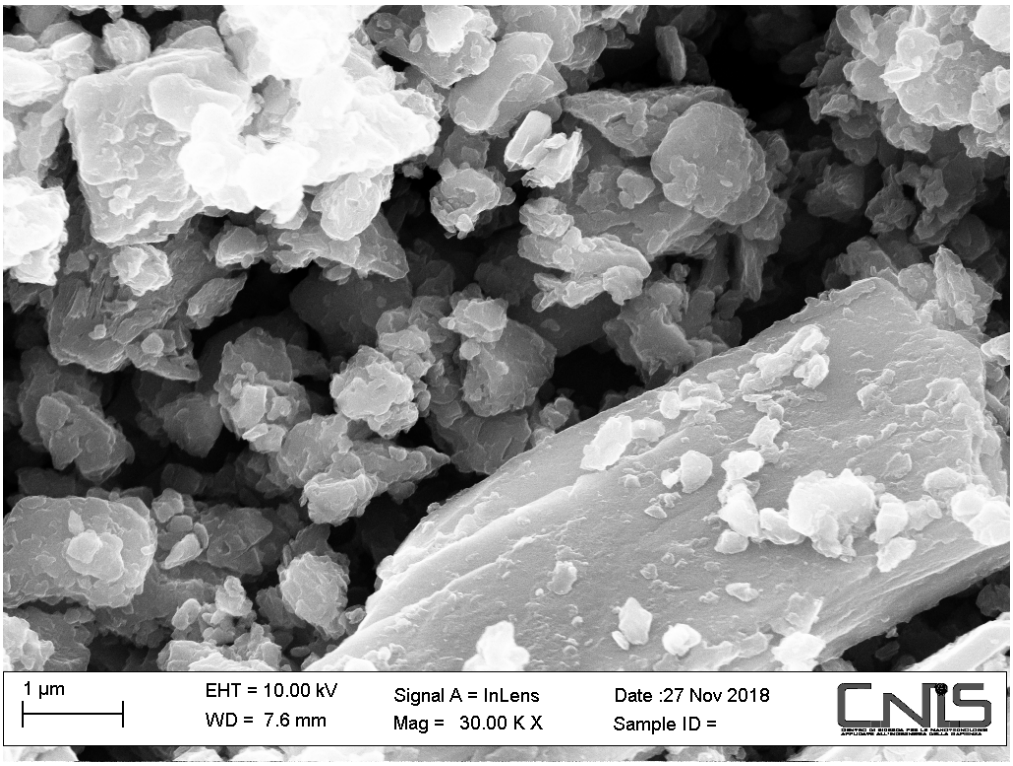

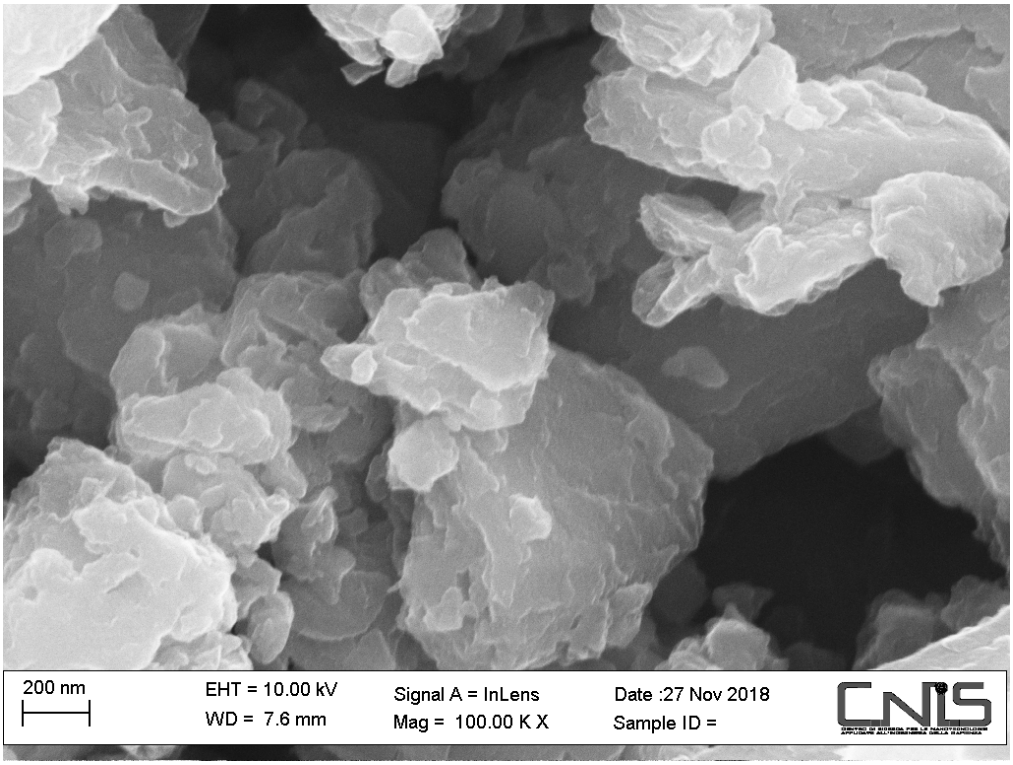
200 nm
EHT = 10.00 kV
WD = 7.6 mm
Signal A = InLens
Mag = 100.00 K X
Date :27 Nov 2018
Sample ID =

*7.2 SEM images of complex **3b***

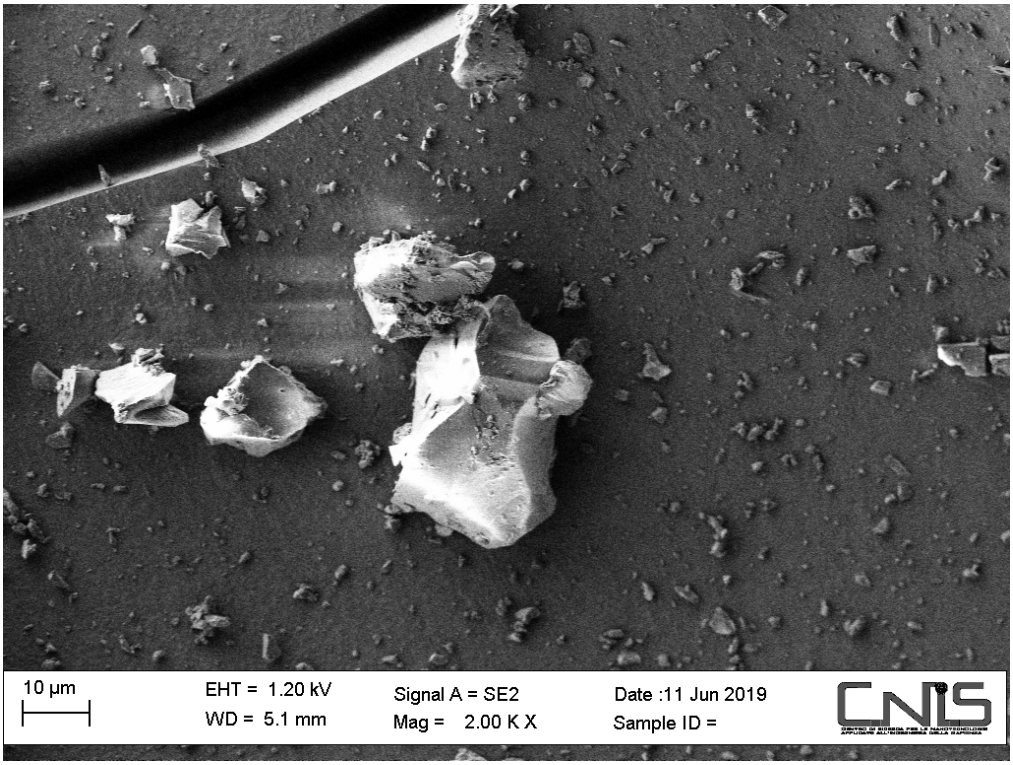

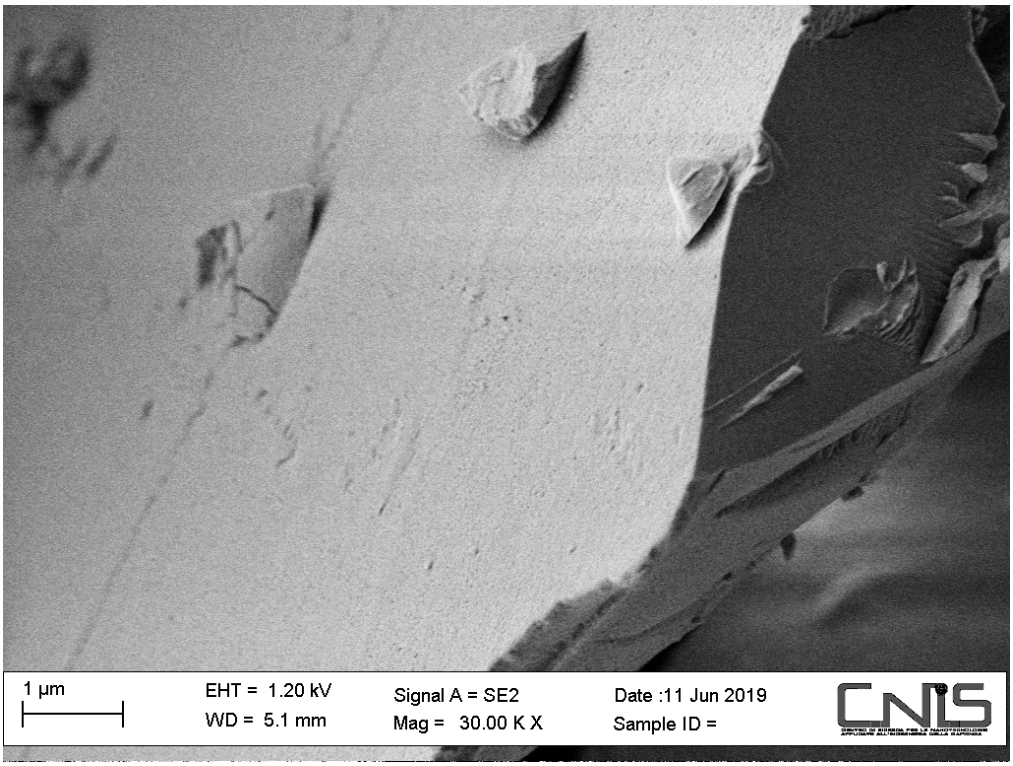

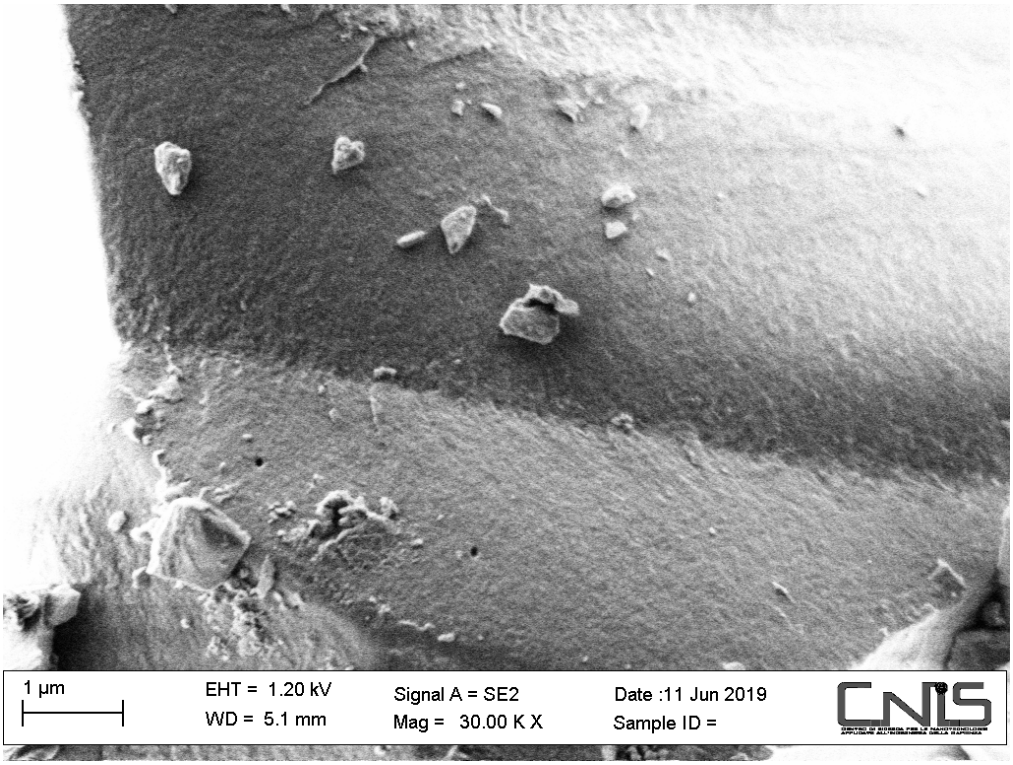
1 µm
EHT = 1.20 kV
WD = 5.1 mm
Signal A = SE2
Mag = 30.00 K X
Date :11 Jun 2019
Sample ID =

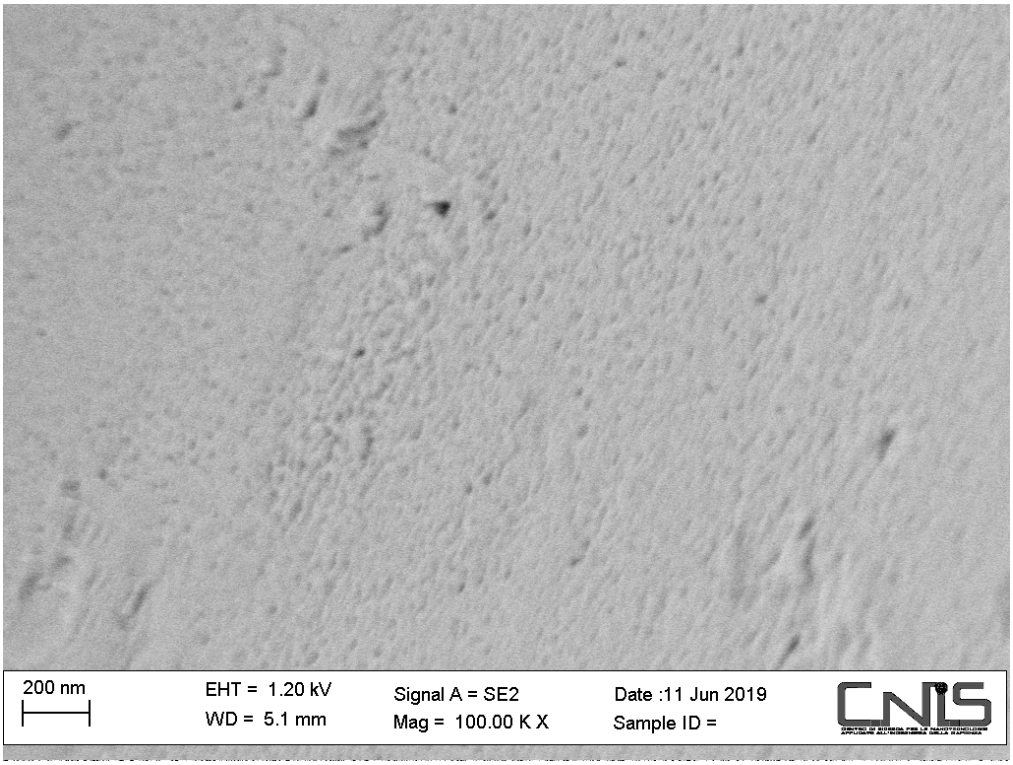
200 nm
EHT = 1.20 kV
WD = 5.1 mm
Signal A = SE2
Mag = 100.00 K X
Date :11 Jun 2019
Sample ID =

*7.3 SEM images of complex **3c***

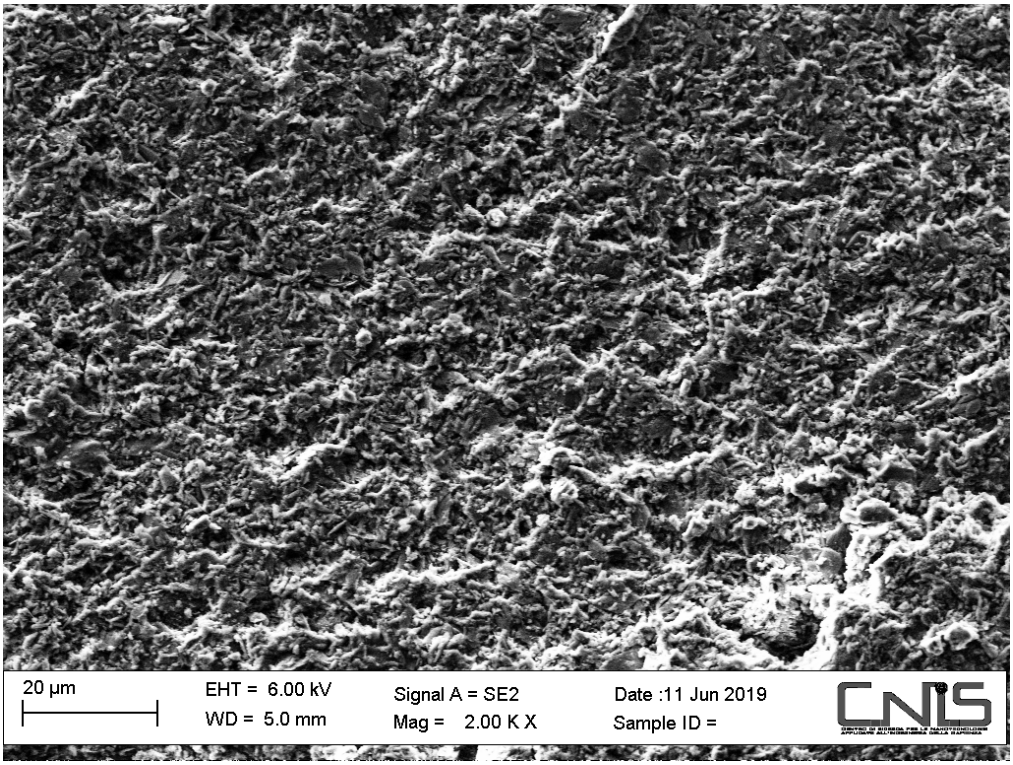

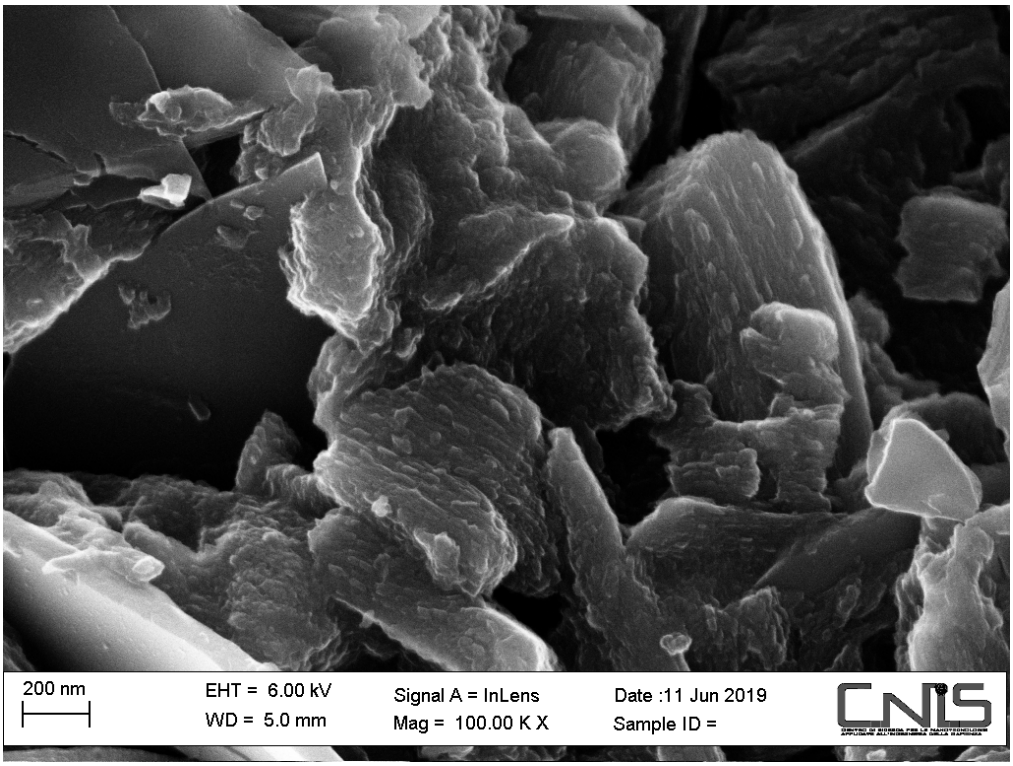

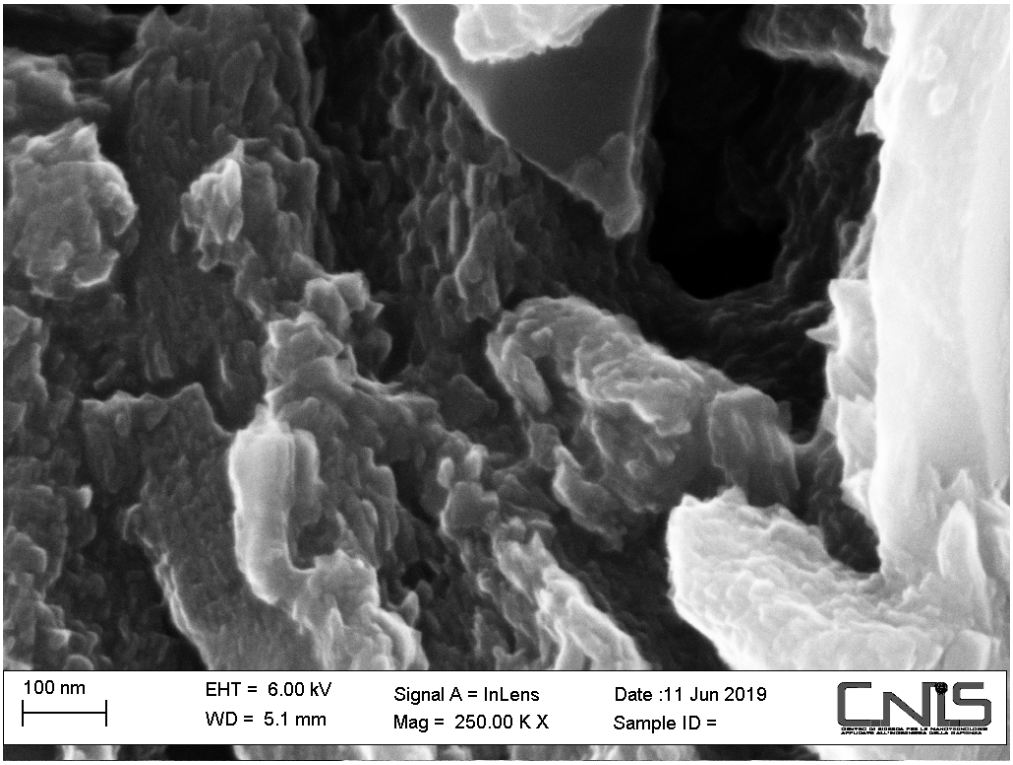
100 nm
EHT = 6.00 kV
WD = 5.1 mm
Signal A = InLens
Mag = 250.00 K X
Date :11 Jun 2019
Sample ID =